Toward RIS-Aided Non-Coherent Communications: A Joint Index Keying M-ary Differential Chaos Shift Keying System

Xiangming Cai, *Member, IEEE*, Chongwen Huang, *Member, IEEE*, Ertugrul Basar, *Fellow, IEEE*, Weikai Xu, *Member, IEEE*, Lin Wang, *Senior Member, IEEE*, Marco Di Renzo, *Fellow, IEEE*, and Chau Yuen, *Fellow, IEEE*

***Abstract*— In reconfigurable intelligent surface (RIS)-aided coherent communications, channel state information (CSI) is often assumed to be perfectly estimated at the receiver. However, perfect CSI cannot be available in practice. Furthermore, the complex and ever-changing channel makes the acquisition of accurate CSI often unaffordable because of the large overhead in transmitting pilot signals. Motivated by these considerations, a novel non-coherent RIS-aided joint index keying M-ary differential chaos shift keying (RIS-JIK-MDCSK) system is proposed in this paper, where the receiver can retrieve information bits by performing non-coherent correlation demodulation without requiring CSI, thereby reducing the system complexity. In RIS-JIK-MDCSK, the states of the reference signal, RIS elements, and information-bearing subcarriers are jointly optimized to devise a joint index keying mechanism, where additional information bits are implicitly transmitted by these state indices, thus increasing the throughput and spectral efficiency. Furthermore, an effective joint index keying detection algorithm is proposed to recover the information bits. The analytical bit error rate (BER) of RIS-JIK-MDCSK is derived over a Rayleigh fading channel. Other evaluation metrics, including the throughput, spectral efficiency, and system complexity are also analyzed and compared against benchmark systems. Numerical simulations are performed to evaluate the superiority of RIS-JIK-MDCSK compared to existing systems.**

***Index Terms*— Non-coherent communications, reconfigurable intelligent surface, M-ary differential chaos shift keying, joint index keying.**

Manuscript received 20 October 2022; revised 11 February 2023; accepted 4 April 2023. Date of publication 24 April 2023; date of current version 12 December 2023. This work was supported in part by the Singapore Ministry of Education Tier 2 under Grant MOE-T2EP50220-0019. The work of Chongwen Huang was supported in part by the China National Key Research and Development Program under Grant 2021YFA1000500, in part by the National Natural Science Foundation of China under Grant 62101492, in part by the Zhejiang Provincial Natural Science Foundation of China under Grant LR22F010002, in part by the National Natural Science Fund for Excellent Young Scientists Fund Program (Overseas), in part by the Zhejiang University Education Foundation Qizhen Scholar Foundation, and in part by the Fundamental Research Funds for the Central Universities under Grant 2021FZZX001-21. The work of Ertugrul Basar was supported by the Scientific and Technological Research Council of Turkey (TUBITAK) under Grant 120E401. The work of Weikai Xu was supported in part by the National Natural Science Foundation of China under Grant 61871337; and in part by the Key Laboratory of Southeast Coast Marine Information Intelligent Perception and Application, Ministry of Natural Resources (MNR), under Grant KFJJ20220201. The work of Lin Wang was supported in part by the National Natural Science Foundation of China under Grant 61671395. The work of Marco Di Renzo was supported in part by the European Commission through the H2020 ARIADNE Project under Grant 871464 and in part by the H2020 RISE-6G Project under Grant 101017011. The associate editor coordinating the review of this article and approving it for publication was W. Chen. *(Corresponding author: Chau Yuen.)*

Xiangming Cai is with the Engineering Product Development Pillar, Singapore University of Technology and Design, Singapore 487372 (e-mail: samson0102@qq.com).

Chongwen Huang is with the College of Information Science and Electronic Engineering, Zhejiang University, Hangzhou 310027, China, also with the International Joint Innovation Center, Zhejiang University, Haining 314400, China, and also with the Zhejiang–Singapore Innovation and AI Joint Research Laboratory and the Zhejiang Provincial Key Laboratory of Information Processing, Communication and Networking (IPCAN), Hangzhou 310027, China (e-mail: chongwenhuang@zju.edu.cn).

Ertugrul Basar is with the Communications Research and Innovation Laboratory (CoreLab), Department of Electrical and Electronics Engineering, Koç University, 34450 Istanbul, Turkey (e-mail: ebasar@ku.edu.tr).

Weikai Xu is with the Department of Information and Communication Engineering, Xiamen University, Xiamen 361005, China, and also with the Key Laboratory of Southeast Coast Marine Information Intelligent Perception and Application, Ministry of Natural Resources (MNR), Zhangzhou 363000, China (e-mail: xweikai@xmu.edu.cn).

Lin Wang is with the Department of Information and Communication Engineering, Xiamen University, Xiamen 361005, China (e-mail: wanglin@xmu.edu.cn).

Marco Di Renzo is with Universite Paris-Saclay, CNRS, CentraleSupelec, Laboratoire des Signaux et Systemes, 91192 Gif-sur-Yvette, France (e-mail: marco.di-renzo@universite-paris-saclay.fr).

Chau Yuen is with the School of Electrical and Electronic Engineering, Nanyang Technological University, Singapore 639798 (e-mail: chau.yuen@ntu.edu.sg).

Color versions of one or more figures in this article are available at https://doi.org/10.1109/TWC.2023.3268071.

Digital Object Identifier 10.1109/TWC.2023.3268071

I. Introduction

THE explosive growth of mobile devices and the ever-increasing demand of ubiquitous wireless communications impose considerable challenges on the fifth-generation and beyond cellular networks. Recently, researchers in wireless communications have expressed keen interests in reconfigurable intelligent surface (RIS)-assisted communications because of their capabilities of improving the bit error rate (BER) in an energy-effective and cost-friendly manner [1], [2], [3], [4]. An RIS is composed of sub-wavelength unit cells with tunable electromagnetic responses, which can be optimized to apply desired transformations to the electromagnetic waves [5]. The amplitude, phase, polarization, and frequency of the impinging signals can be deliberately controlled by external signals in a real-time and reconfigurable manner to enhance the signal quality at the receiver [6], [7].

RISs have gained significant interest from many research communities. Specifically, the employment of an RIS as an access point (AP) was proposed in [8], where it was demonstrated that an RIS-aided AP system is capable of obtaining superior BER performance even for low values of the signal-to-noise ratio (SNR). Furthermore, based on the RIS-assisted indexing mechanism, RIS-based space shift keying (RIS-SSK) and RIS-based spatial modulation (RIS-SM) systems were proposed in [9]. Moreover, two RIS-assisted SM systems were proposed in [10], where the power allocation matrix at the transmitter and the reflection coefficients at the RIS are jointly optimized to improve the system reliability. An RIS-aided beam index modulation system was proposed in [11], where the usage of an RIS is shown to reduce the cost of beamforming since additional bits are transmitted by beam index modulation without inducing extra cost. Recently, an RIS-assisted receive quadrature space shift keying system was proposed in [12], where the real and imaginary dimensions are independently used for index modulation (IM) to enhance the spectral efficiency. Also, an RIS grouping-based IM system was proposed in [13], where the RIS is divided into several group-surfaces (GR), and the index of a GR is used to transmit additional information bits, thereby improving the spectral efficiency.

In the aforementioned RIS-aided systems, it is assumed that perfect channel state information (CSI) is available at the receiver. However, the BER of coherent RIS-aided communication systems heavily depends on the quality of CSI. Although there are some works, such as [14] and [15], devoted to designing low-overhead channel estimation strategies for RIS-aided systems, the acquisition of accurate CSI is quite challenging in practice because of the nearly-passive design constraints of RISs. To avoid the transmission of pilot signals and channel estimation, non-coherent communications can be utilized. There exist two distinct approaches for non-coherent communications. One approach exploits the correlation between consecutive received signals such that information bits can be retrieved in a non-coherent manner [16]. Another approach is based on energy detection, which significantly reduces the pilot training overhead and simplifies the receiver design at the cost of degrading the system performance [17].

As a promising correlation-based non-coherent system, the differential chaos shift keying (DCSK) system exploits a correlation receiver to avoid the use of CSI and the reproduction of chaotic signals at the receiver, while providing good performance over fading channels [18], [19]. Therefore, DCSK-based systems have been widely studied for application to many scenarios [20], [21], [22], [23], [24], [25]. It is worth noting that the DCSK system exploits the transmitted reference approach to alleviate the adverse effect of channel fading, which means that DCSK transmits a reference sequence appended to the information-bearing sequence. However transmitted reference systems incur two major disadvantages (i) low energy and spectral efficiency; (ii) BER performance degradation due to the presence of noise in the reference signal.

To address the first disadvantage of DCSK, a multi-carrier DCSK (MC-DCSK) system was proposed in [26], where a reference signal is shared with multiple information-bearing signals, thereby enhancing the energy efficiency. Furthermore, a reference-free DCSK system was proposed in [27], where the reference signal is removed and information bits are implicitly transmitted by code-shifted indices. Recently, deep learning-aided DCSK was proposed in [28], where the features of the chaotic sequence are learned off-line to formulate the optimal de-mapping such that the reference signal can be exempted and energy efficiency is enhanced. To deal with the second disadvantage, different noise suppression techniques were developed and applied in DCSK-based systems to enhance their BER performance [29], [30], [31].

As an energy-efficient and promising technology, index modulation is capable of utilizing the indices of physical features of communication systems to convey additional information bits [32]. IM systems have the ability to realize new modulation systems with better BER performance [33]. Benefiting from these advantages of IM, a carrier index DCSK (CI-DCSK) system was proposed in [34] and then optimized leading to the generalized CI-DCSK (GCI-DCSK) [35] and carrier index M-ary DCSK (CI-MDCSK) [36] systems. Also, code index modulation (CIM) technology was used in [37] to devise a CIM-based multi-carrrier M-ary DCSK (CIM-MC-MDCSK) system for better BER performance. In IM-based DCSK systems, the indices of Walsh codes [37], [38], permutation patterns [39], [40], modulation types [41], [42], and space-time matrices [43] are also utilized as dimensions for the transmission of additional information bits. Furthermore, multidimensional IM technology was integrated into DCSK to further increase the data rate and energy efficiency [44], [45].

To avoid the overhead of pilot signals and complex channel estimation in coherent RIS-aided systems, and enhance the throughput, spectral efficiency, and BER performance of DCSK, a non-coherent RIS-aided joint index keying M-ary differential chaos shift keying (RIS-JIK-MDCSK) system is proposed in this paper. In the proposed RIS-JIK-MDCSK system, the states of the reference signal, RIS elements, and information-bearing subcarriers are jointly optimized to devise a joint index keying mechanism, where additional bits are implicitly transmitted by these state indices, thus enhancing the throughput and spectral efficiency. The proposed joint index keying mechanism includes the reference keying, RIS keying, and carrier keying. To the best of our knowledge, this is one of the first works that investigates RIS-aided non-coherent chaotic communication systems.

The main contributions of this paper are summarized as follows:

1) We propose a non-coherent RIS-JIK-MDCSK system, where an RIS-aided joint index keying mechanism is devised to achieve high throughput and superior BER performance, and the transmitted reference structure of the proposed system enables the receiver to recover information bits without requiring expensive channel estimation.
2) We propose an effective joint index keying detection algorithm to retrieve the information bits transmitted by the state indices of the reference signal, RIS elements, and information-bearing subcarriers, and physically modulated M-ary phase shift keying (M-PSK) symbols.
3) We derive the error probability of the information bits transmitted by the modulated M-PSK symbols, the

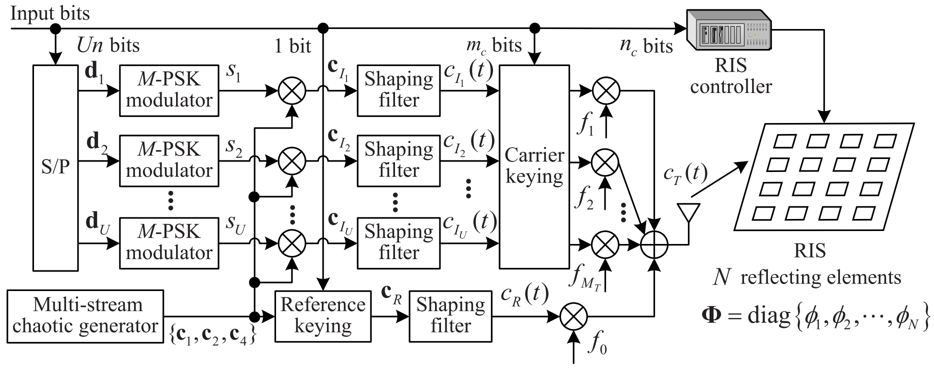

Fig. 1. Block diagram of the proposed RIS-JIK-MDCSK transmitter.

probabilities of correct reference keying, RIS keying, and carrier keying detections. Also, the BER performance, throughput, spectral efficiency, and system complexity of the proposed RIS-JIK-MDCSK system are analyzed.

4) We carry out BER performance simulations for RIS-JIK-MDCSK to verify the correctness of the proposed analytical BER expressions. We also compare the throughput, spectral efficiency, and BER performance of the proposed RIS-JIK-MDCSK system against other benchmark systems to evaluate the superiority of RIS-JIK-MDCSK.

The rest of this paper are organized as follows. The system model of the proposed RIS-JIK-MDCSK system and the proposed joint index keying detection algorithm are introduced in Section II. The BER performance analysis of RIS-JIK-MDCSK is given in Section III. Then, the throughput, spectral efficiency, and system complexity of RIS-JIK-MDCSK are analyzed in Section IV. Furthermore, numerical results and discussions are presented in Section V. Finally, Section VI concludes the paper.

II. The Proposed RIS-JIK-MDCSK System

In this section, we present the proposed RIS-JIK-MDCSK transmitter and receiver, and elaborate their operating principles. Furthermore, the proposed joint index keying detection algorithm is presented in this section.

A. The Proposed RIS-JIK-MDCSK Transmitter

Fig. 1 shows the block diagram of the RIS-JIK-MDCSK transmitter. The input bits are split into four parts, including one reference keying bit, n_c RIS keying bits, m_c carrier keying bits, and Un physically modulated bits, where U is the number of activated information-bearing carriers and $n = \log_2 M$ is the number of information bits carried by an M-PSK symbol. Therefore, the total number of transmitted bits by an RIS-JIK-MDCSK symbol is given by $\partial = 1 + n_c + m_c + Un$.

At the transmitter, we propose a multi-stream chaotic generator to generate different chaotic signals. The block diagram of the proposed multi-stream chaotic generator is shown in Fig. 2. The initial normalized chaotic signal

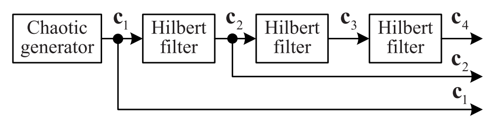

Fig. 2. Block diagram of the proposed multi-stream chaotic generator.

$\mathbf{c}_1 = [c_{1,1}, c_{1,2}, \ldots, c_{1,\beta}]$ is generated by a chaotic generator, where the second-order Chebyshev polynomial function, i.e., $c_k = 2c_{k-1}^2 - 1, k = 1, 2, \ldots, \beta$, is used [46], [47]. Since $\mathbf{c}_1$ is a length-β normalized chaotic signal, it holds $\mathbf{c}_1(\mathbf{c}_1)^T = 1$. The chaotic signal $\mathbf{c}_1$ is arranged to generate pair-orthogonal signals by performing the discrete Hilbert transform several times, as shown in Fig. 2. Thus, the i-th chaotic signal $\mathbf{c}_i$ is given by

$$\mathbf{c}_i = \mathcal{H}_{i-1}(\mathbf{c}_1), i = 2, 3, 4, \tag{1}$$

where $\mathcal{H}_{i-1}(\cdot)$ denotes the discrete Hilbert transformation [48], which is performed for $(i-1)$ times. It is worth mentioning that only $\mathbf{c}_1$, $\mathbf{c}_2$, and $\mathbf{c}_4$ are used at the RIS-JIK-MDCSK transmitter. The chaotic signal $\mathbf{c}_1$ and its Hilbert transform $\mathcal{H}(\mathbf{c}_1)$, i.e., $\mathbf{c}_2$, are orthogonal to each other. Therefore, we have $\mathbf{c}_1(\mathcal{H}(\mathbf{c}_1))^T = \mathbf{c}_1(\mathbf{c}_2)^T = 0$. In addition, by utilizing the inversion property of the discrete Hilbert transform, i.e., $\mathcal{H}(\mathcal{H}(\mathbf{c}_1)) = -\mathbf{c}_1$, we obtain

$$\begin{aligned}\mathbf{c}_1(\mathbf{c}_4)^T &= \mathbf{c}_1[\mathcal{H}_3(\mathbf{c}_1)]^T = \mathbf{c}_1[\mathcal{H}(\mathcal{H}(\mathcal{H}(\mathbf{c}_1)))]^T \\ &= \mathbf{c}_1[-\mathcal{H}(\mathbf{c}_1)]^T = -\mathbf{c}_1(\mathbf{c}_2)^T = 0.\end{aligned} \tag{2}$$

The proof for the inversion property of the discrete Hilbert transform can be given as

$$\begin{aligned}\mathcal{F}(\mathcal{H}(\mathcal{H}(\mathbf{c}_1))) &= [-\jmath\text{sgn}(\omega)]\mathcal{F}(\mathcal{H}(\mathbf{c}_1)) \\ &= [-\jmath\text{sgn}(\omega)][-\jmath\text{sgn}(\omega)]\mathcal{F}(\mathbf{c}_1) \\ &= \jmath^2[\text{sgn}(\omega)]^2\mathcal{F}(\mathbf{c}_1) \\ &= -\mathcal{F}(\mathbf{c}_1) = \mathcal{F}(-\mathbf{c}_1),\end{aligned} \tag{3}$$

where $\mathcal{F}(\cdot)$ denotes the discrete Fourier transform (DFT) operation, $\jmath$ is the imaginary unit, and $\text{sgn}(\cdot)$ denotes the sign function. According to (3), $\mathcal{H}(\mathcal{H}(\mathbf{c}_1))$ and $-\mathbf{c}_1$ have the same discrete Fourier transform, and thus we can conclude $\mathcal{H}(\mathcal{H}(\mathbf{c}_1)) = -\mathbf{c}_1$.

Generally, the operation at the RIS-JIK-MDCSK transmitter can be divided into four parts, including reference keying

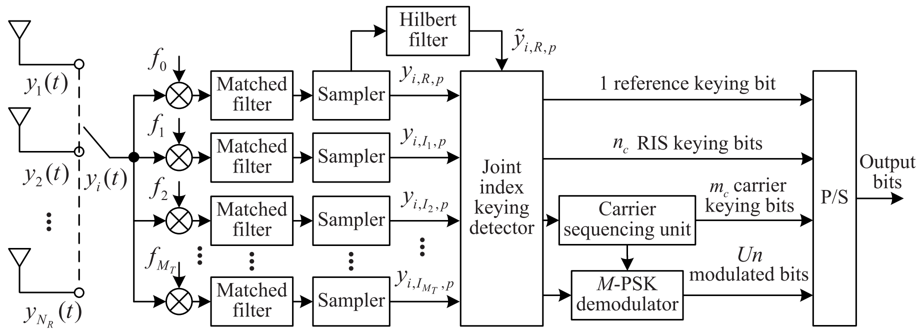

Fig. 3. Block diagram of the proposed RIS-JIK-MDCSK receiver.

modulation, carrier keying modulation, chaos-based M-PSK modulation, and RIS keying modulation, respectively. The operation of each component is elaborated as follows.

1) Reference Keying Modulation: Differently from conventional DCSK-based systems, where the reference signal does not transmit information bits, we propose a reference keying mechanism for the RIS-JIK-MDCSK system, which transmits one information bit by selecting the desired reference signal. Note that one reference keying bit, denoted by d_r, is transmitted such that only two orthogonal chaotic signals are required. In this case, the reference keying modulation can be formulated as

$$\mathbf{c}_R = \begin{cases} \mathbf{c}_1,\ d_r = 1 \\ \mathbf{c}_4,\ d_r = 0 \end{cases}, \tag{4}$$

where $\mathbf{c}_R$ is the resultant reference signal. Then, the discrete signal $\mathbf{c}_R$ is transformed into an analog signal by a pulse shaping filter with sampling duration T_c, and the corresponding analog signal is given by

$$c_R(t) = \sum_{p=1}^{\beta} c_{R,p} \hbar(t - pT_c), \tag{5}$$

where $c_{R,p}$ is the p-th element of $\mathbf{c}_R$ and $\hbar(t)$ denotes the normalized impulse response of the shaping filter.

2) Carrier Keying Modulation: There are M_T+1 subcarriers in RIS-JIK-MDCSK, where one of them is arranged to transmit the reference signal and M_T subcarriers are used to carry the information-bearing signals. Note that only U out of M_T information-bearing subcarriers are activated and the remaining $M_T - U$ carriers are idle. Accordingly, the number of carrier keying bits is $m_c = \lfloor \log_2 C_{M_T}^U \rfloor$, where $C_{M_T}^U = \frac{M_T!}{U!(M_T-U)!}$ is the binomial coefficient and $\lfloor \cdot \rfloor$ denotes the floor function. Generally, lookup tables and combinatorial methods can be applied in the carrier keying selection [49]. The carrier keying vector is defined as $\mathbf{w} = [w_1, w_2, \ldots, w_{M_T}]$, where U elements of $\mathbf{w}$ are equal to 1, which correspond to the U information-bearing activated subcarriers, and $M_T - U$ elements are equal to 0, which correspond to the inactivated subcarriers.

3) Chaos-Based M-PSK Modulation: The Un physically modulated bits, expressed in a vector form as $[\mathbf{d}_1, \mathbf{d}_2, \ldots, \mathbf{d}_U]$, can be divided into U sub-blocks with each sub-block containing n modulated bits. When the u-th sub-block of modulated bits is mapped onto the M-ary constellation, it gives $s_u = a_u + \jmath b_u$, where a_u and b_u denote the real and imaginary parts of the M-PSK symbol s_u, respectively. After modulation, the chaotic signals $\mathbf{c}_1$ and $\mathbf{c}_2$ are exploited to carry the u-th M-PSK symbol, yielding

$$\mathbf{c}_{I_u} = a_u \mathbf{c}_1 + \jmath b_u \mathbf{c}_2, u = 1, 2, \ldots, U, \tag{6}$$

where $\mathbf{c}_{I_u}$ is the resultant u-th information-bearing signal. Using the pulse shaping filter, the discrete information-bearing signals are converted into analog signals as follows

$$c_{I_u}^{\Re}(t) = \sum_{p=1}^{\beta} (c_{I_u,p})_{\Re} \hbar(t - pT_c), \tag{7}$$

$$c_{I_u}^{\Im}(t) = \sum_{p=1}^{\beta} (c_{I_u,p})_{\Im} \hbar(t - pT_c), \tag{8}$$

where $(\cdot)_{\Re}$ and $(\cdot)_{\Im}$ denote the real and imaginary operations, respectively. $c_{I_u,p}$ is the p-th element of $\mathbf{c}_{I_u}$. The analog reference and information-bearing signals are transmitted by different subcarriers with the aid of the carrier keying vector $\mathbf{w}$. Therefore, the signal transmitted from the transmit antenna to the RIS can be formulated as

$$\begin{aligned} c_T(t) &= c_R(t)\cos(2\pi f_0 + \iota_0) \\ &\quad + \sum_{u=1}^{M_T} w_u \big[c_{I_u}^{\Re}(t)\cos(2\pi f_u + \iota_u) \\ &\quad + c_{I_u}^{\Im}(t)\sin(2\pi f_u + \iota_u)\big], \end{aligned} \tag{9}$$

where f_u and ι_u are the frequency and initial phase of the u-th subcarrier, respectively.

4) RIS Keying Modulation: An RIS equipped with N nearly passive reflecting elements is deployed at the transmitter, and the reflection phase matrix of the RIS is represented as $\mathbf{\Phi} = \mathrm{diag}\{\phi_1, \phi_2, \ldots, \phi_N\}$, where ϕ_k denotes the phase of the k-th RIS element that lies in the set $(0, 2\pi)$. It is assumed that the radio frequency (RF) signals reflected by each element of the RIS are independent of each other, and therefore the electromagnetic mutual coupling among the RIS elements can be ignored. The RIS is deployed as a part of the transmitter such that the transmit antenna is close enough to it. Therefore, the channel fading between the transmit antenna and the RIS can be ignored [8]. In the proposed RIS-JIK-MDCSK system, N_R receive antennas are used at the receiver, and the received signal is maximized at only one of the N_R receive antennas, depending on the $n_c = \lfloor \log_2 N_R \rfloor$ bits. Therefore, the n_c bits depend on the number of available receive antennas.

Specifically, the maximum SNR at the desired receive antenna is obtained by adjusting the phases of the RIS elements to be equal to the channel phases, where the channel is the one between the RIS and the desired receive antenna. From this perspective, the phases of the RIS depend on the n_c RIS keying bits that maximize the received SNR at the desired receive antenna. Therefore, the RF signal reflected from the RIS is expressed as

$$x_k\left(t\right) = g_k c_T\left(t\right) = \alpha_k e^{\jmath\phi_k} c_T\left(t\right), \tag{10}$$

where $g_k = \alpha_k e^{\jmath\phi_k}$ is the reflection coefficient of the k-th RIS element, and α_k and ϕ_k are the amplitude and phase of the k-th RIS element, respectively. It is assumed that the reflection coefficient of RIS elements is normalized, i.e., $\alpha_k = 1$, for simplicity.

B. The Proposed RIS-JIK-MDCSK Receiver

The block diagram of the RIS-JIK-MDCSK receiver is illustrated in Fig. 3. At the receiver, N_R antennas are available, and the received signal at the i-th antenna can be represented as

$$y_i\left(t\right) = \sum_{k=1}^{N}\left[h_{i,k}\left(t\right) * x_k\left(t\right)\right] + n_i\left(t\right), \tag{11}$$

where $*$ denotes the convolution operation, $h_{i,k}(t)$ is the impulse response of the fading channel, whose discrete counterpart is expressed as $h_{i,k} = \chi_{i,k} e^{-\jmath\psi_{i,k}}, i = 1, 2, \ldots, N_R, k = 1, 2, \ldots, N$. Here, $\chi_{i,k}$ and $\psi_{i,k}$ denote the channel coefficient and phase between the i-th receive antenna and the k-th RIS element, respectively. Moreover, $h_{i,k}$ follows a complex Gaussian distribution $\mathcal{CN}(0, \sigma^2)$ and $\psi_{i,k}$ is uniformly distributed in $(0, 2\pi)$. Furthermore, $n_i(t)$ is the complex additive white Gaussian noise (AWGN) with zero mean and N_0 variance.

To retrieve the ∂ information bits, the RIS-JIK-MDCSK system first needs to estimate the reference signal that is used for the reference keying and the phase shift of the RIS by identifying the receive antenna where the SNR is maximized. Therefore, one reference keying bit and n_c RIS keying bits are recovered by identifying the indices of the reference keying and RIS keying modulation, respectively. Following the first step, the carrier keying bits can be first recovered by the carrier sequencing unit that determines the indices of the activated subcarriers, and then the physically transmitted bits carried by the activated subcarriers can be demodulated by the M-PSK demodulator. Since the N_R receive antennas operate independently of each other, we only describe the information recovery process of the received signal for the i-th receive antenna for simplicity.

For the i-th receive antenna, the synchronized orthogonal subcarriers are exploited to demodulate the reference and information-bearing signals. The resultant analog signals are processed by the matched filters and samplers to obtain the corresponding discrete signals. Generally, the discrete reference signal and the u-th discrete information-bearing signal are formulated as

$$y_{i,R,p} = \sum_{k=1}^{N} h_{i,k} e^{\jmath\phi_k} c_{R,p} + n_{R,p}, \tag{12}$$

$$y_{i,I_u,p} = \sum_{k=1}^{N} h_{i,k} e^{\jmath\phi_k} c_{I_u,p} + n_{I_u,p}, \tag{13}$$

Algorithm 1 Joint Index Keying Detection Algorithm

Input: $y_{i,R,p}$, $\tilde{y}_{i,R,p}$, and $y_{i,I_u,p}$;
for $i = 1, 2, \ldots, N_R$ **do**
  for $u = 1, 2, \ldots, M_T$ **do**
    $D_{\Re} = \sum_{p=1}^{\beta}(y_{i,R,p})_{\Re}(y_{i,I_u,p})_{\Re}$;
    $D_{\Im} = \sum_{p=1}^{\beta}(\tilde{y}_{i,R,p})_{\Re}(y_{i,I_u,p})_{\Im}$;
    $D_{i,u} = D_{\Re} + \jmath D_{\Im}$;
    $G_{\Re} = \sum_{p=1}^{\beta}(\tilde{y}_{i,R,p})_{\Re}(y_{i,I_u,p})_{\Re}$;
    $G_{\Im} = \sum_{p=1}^{\beta}(y_{i,R,p})_{\Re}(y_{i,I_u,p})_{\Im}$;
    $G_{i,u} = G_{\Re} + \jmath G_{\Im}$;
  end
end
Obtain the maximum of $|D_{i,u}|$, i.e., D_m, and record the row index I_{Dr} and column index I_{Dc} of D_m;
Obtain the maximum of $|G_{i,u}|$, i.e., G_m, and record the row index I_{Gr} and column index I_{Gc} of G_m;
if $D_m > G_m$ **then**
  Estimate the reference keying bit as $d_r = 1$;
  Estimate the RIS keying index that maximizes the SNR of the $\hat{i}$-th receive antenna, i.e., $\hat{i} = I_{Dr}$;
  Obtain the decision variables for carrier keying detection by $K = D_{I_{Dr},u}, u = 1, 2, \ldots, M_T$;
else
  Estimate the reference keying bit as $d_r = 0$;
  Estimate the RIS keying index that maximizes the SNR of the $\hat{i}$-th receive antenna, i.e., $\hat{i} = I_{Gr}$;
  Obtain the decision variables for carrier keying detection by $K = G_{I_{Gr},u}, u = 1, 2, \ldots, M_T$;
end
Convert the estimated RIS keying index, $\hat{i} - 1$, into binary numbers and retrieve n_c RIS keying bits;
Find the U maximum values of $|K|$ and sort the indices of these maximum values in a descend sequence to estimate $\{\upsilon_U, \upsilon_{U-1}, \ldots, \upsilon_1\}$, $\upsilon_U > \upsilon_{U-1} > \ldots > \upsilon_1$;
Convert J into binary numbers and retrieve m_c carrier keying bits, where $J = \sum_{u=1}^{U} C_{\upsilon_u}^{u}$;
for $u = 1, 2, \ldots, U$ **do**
  Perform the M-PSK demodulation based on $\hat{K}(\upsilon_u)$ and recover the u-th sub-block of modulated bits;
end
Combine the U sub-block of modulated bits to estimate all Un modulated bits;
Output: One reference keying bit, n_c RIS keying bits, m_c carrier keying bits, and Un physically modulated bits.

where $n_{R,p}$ and $n_{I_u,p}$ denote the discrete complex AWGN, imposed on the reference signal and the u-th information-bearing signal, respectively. The orthogonal signal of the reference signal is obtained by performing the discrete Hilbert transformation on $y_{i,R,p}$, yielding

$$\tilde{y}_{i,R,p} = \mathcal{H}_1\left(y_{i,R,p}\right) = \sum_{k=1}^{N} h_{i,k} e^{\jmath\phi_k} \tilde{c}_{R,p} + \tilde{n}_{R,p}, \tag{14}$$

where $\tilde{c}_{R,p}$ and $\tilde{n}_{R,p}$ are the orthogonal versions of $c_{R,p}$ and $n_{R,p}$, respectively. In (14), we use the operation $\mathcal{H}_1(\cdot)$ to obtain the orthogonal signal of $y_{i,R,p}$, rather than $\mathcal{H}_3(\cdot)$, because $\mathcal{H}_1(\cdot)$ only needs to perform the discrete Hilbert transform once, while $\mathcal{H}_3(\cdot)$ needs to perform the discrete Hilbert transform three times. In this case, the complexity of $\mathcal{H}_1(\cdot)$ is generally lower than that of $\mathcal{H}_3(\cdot)$.

Generally, maximum likelihood (ML) detection can be applied to retrieve the reference keying bit and RIS keying bits, but the performance of this approach is severely dependent on the quality of channel estimation. In addition, the searching process of ML detection for all combinations of the receive antennas, reference signals, activated subcarriers, and M-PSK symbols suffers from overwhelming computational complexity especially in the case of a larger number of RIS elements, subcarriers, and antennas. Therefore, a practical non-coherent joint index keying detection algorithm is developed to ease the computational complexity of ML detection. It is worth noting that the proposed joint index keying detection algorithm is a correlation-based detection method, where the information bits can be retrieved by using the correlation between the reference and information-bearing signals, thereby avoiding the use of channel estimation at the RIS-JIK-MDCSK receiver.

The pseudo-code of the proposed algorithm is shown in Algorithm 1, which is initialized by $y_{i,R,p}$, $\tilde{y}_{i,R,p}$, and $y_{i,I_u,p}$, $i = 1, 2, \ldots, N_R, u = 1, 2, \ldots, U$. From Line 4 to Line 6, the reference signal and its discrete Hilbert transform signal are correlated with the information-bearing signals, and the resultant decision variable is given by (15), as shown at the bottom of the page. Similarly, when the correlation order is changed reversely, another decision variable $G_{i,u}$ is obtained in (16), as shown at the bottom of the page. Note that the two decision variables are obtained by means of different reference signals such that the reference keying bit can be estimated based on the magnitude of D_m and G_m as shown in Lines 15 and 19. Furthermore, if $D_m > G_m$, the RIS keying index that maximizes the received SNR of the $\hat{i}$-th receive antenna is estimated as $\hat{i} = I_{Dr}$, otherwise it is estimated as $\hat{i} = I_{Gr}$. Then, n_c RIS keying bits can be recovered by converting the estimated index $\hat{i} - 1$ into bits. In Line 24, the algorithm searches for U maximum values out of $|K|$ and the indices of these maxima are used to recover the m_c carrier keying bits as shown in Line 25. Note that $C_{v_u}^{u}$ in Line 25 is the binomial coefficient, i.e., $C_{v_u}^{u} = \frac{v_u!}{u!(v_u-u)!}$. The physically modulated bits are estimated based on $\hat{K}(v_u)$, where $\hat{K}$ is a modified version of K, given by

$$\hat{K} = \begin{cases} (K)_{\Re} + \jmath(K)_{\Im}, & d_r = 1 \\ (K)_{\Re} - \jmath(K)_{\Im}, & d_r = 0 \end{cases}. \tag{17}$$

Then, the transmitted M-PSK symbol can be estimated by the minimum distance decision criterion, given by $\hat{s}_u = \arg\min(|\hat{K} - s_u|^2), s_u \in S, u = 1, 2, \ldots, U$, where S denotes the M-PSK constellation symbol set and s_u is the u-th M-PSK constellation symbol in the set S. After converting the estimated M-PSK symbol $\hat{s}_u$ into binary bits, the u-th sub-block of physically modulated bits is retrieved. Finally, the Un physically modulated bits can be obtained by combining U sub-blocks of modulated bits in Line 29.

Remark 1: As shown in Algorithm 1, the proposed detection algorithm retrieves the reference keying bit first, followed by the RIS keying bits, the carrier keying bits, and finally the physically modulated bits. Therefore, an incorrect reference keying detection would result in an incorrect RIS keying detection and an incorrect carrier keying detection. Furthermore, an incorrect RIS keying detection would lead to an incorrect carrier keying detection.

$$\begin{aligned} D_{i,u} &= \sum_{p=1}^{\beta} (y_{i,R,p})_{\Re} (y_{i,I_u,p})_{\Re} + \jmath \sum_{p=1}^{\beta} (\tilde{y}_{i,R,p})_{\Re} (y_{i,I_u,p})_{\Im} \\ &= \sum_{p=1}^{\beta} \left[\sum_{k=1}^{N} h_{i,k} e^{\jmath\phi_k} c_{R,p} + n_{R,p} \right]_{\Re} \left[\sum_{k=1}^{N} h_{i,k} e^{\jmath\phi_k} \left(a_u c_{1,p} + \jmath b_u c_{2,p}\right) + n_{I_u,p} \right]_{\Re} \\ &\quad + \jmath \sum_{p=1}^{\beta} \left[\sum_{k=1}^{N} h_{i,k} e^{\jmath\phi_k} \tilde{c}_{R,p} + \tilde{n}_{R,p} \right]_{\Re} \left[\sum_{k=1}^{N} h_{i,k} e^{\jmath\phi_k} \left(a_u c_{1,p} + \jmath b_u c_{2,p}\right) + n_{I_u,p} \right]_{\Im}. \end{aligned} \tag{15}$$

$$\begin{aligned} G_{i,u} &= \sum_{p=1}^{\beta} (\tilde{y}_{i,R,p})_{\Re} (y_{i,I_u,p})_{\Re} + \jmath \sum_{p=1}^{\beta} (y_{i,R,p})_{\Re} (y_{i,I_u,p})_{\Im} \\ &= \sum_{p=1}^{\beta} \left[\sum_{k=1}^{N} h_{i,k} e^{\jmath\phi_k} \tilde{c}_{R,p} + \tilde{n}_{R,p} \right]_{\Re} \left[\sum_{k=1}^{N} h_{i,k} e^{\jmath\phi_k} \left(a_u c_{1,p} + \jmath b_u c_{2,p}\right) + n_{I_u,p} \right]_{\Re} \\ &\quad + \jmath \sum_{p=1}^{\beta} \left[\sum_{k=1}^{N} h_{i,k} e^{\jmath\phi_k} c_{R,p} + n_{R,p} \right]_{\Re} \left[\sum_{k=1}^{N} h_{i,k} e^{\jmath\phi_k} \left(a_u c_{1,p} + \jmath b_u c_{2,p}\right) + n_{I_u,p} \right]_{\Im}. \end{aligned} \tag{16}$$

TABLE I
DIFFERENT EVENTS, THE CORRESPONDING MEANINGS, AND THEIR OCCURRENCE PROBABILITIES

Event	Meaning	Probability
A	Correct reference keying detection	P_A
A'	Incorrect reference keying detection	$P_{A'}$
B	Correct RIS keying detection	P_B
B'	Incorrect RIS keying detection	$P_{B'}$
C	Correct carrier keying detection	P_C
C'	Incorrect carrier keying detection	$P_{C'}$

III. BER PERFORMANCE ANALYSIS

In this section, we analyze the BER performance of the proposed RIS-JIK-MDCSK system. Since the RIS-JIK-MDCSK receiver includes reference keying detection, RIS keying detection, and carrier keying detection, their detection probabilities are analyzed. For the convenience of analysis, Table I shows different detection events and the corresponding probabilities. For example, the event that the reference keying is detected correctly is termed as A and its occurrence probability is P_A, and the opposite event is denoted by A' with occurrence probability $P_{A'}$. Therefore, under the condition that events A, B, and C occur, we define P_{cm} as the BER of physically modulated bits.

A. The BER of Modulated Bits Under the Condition That Events A, B, and C Occur

When the events A, B, and C occur, the reference keying, RIS keying, and carrier keying are correctly detected such that the phase shift of the RIS is set to $\phi_k = \psi_{\hat{i},k}$ to maximize the received SNR of the $\hat{i}$-th receive antenna. Without loss of generality, it is assumed that $\mathbf{c}_1$ is transmitted as the reference signal, i.e., $\mathbf{c}_R = \mathbf{c}_1$. Therefore, the decision variable obtained from (15) can be simplified as (18), as shown at the bottom of the page. In (18), $n^{\Re}_{I_u,p}$ and $n^{\Im}_{I_u,p}$ denote the real and imaginary parts of $n_{I_u,p}$, respectively. In addition, $\tilde{c}_{R,p}$ can be obtained by computing the discrete Hilbert transform for once on $c_{1,p}$, which yields $\tilde{c}_{R,p} = c_{2,p}$. Note that $\chi_{\hat{i},k}$ is a Rayleigh-distributed variable with mean $\frac{\sqrt{\pi}}{2}$ and variance $\frac{4-\pi}{4}$. According to the central limit theorem, the variable $\sum_{k=1}^{N}\chi_{\hat{i},k}$ has a Gaussian distribution $\mathcal{N}(\frac{N\sqrt{\pi}}{2}, \frac{N(4-\pi)}{4})$ for large values of N [50].

The real part of $D_{\hat{i},u}$, i.e., $D^{\Re}_{\hat{i},u}$, is rewritten as

$$D^{\Re}_{\hat{i},u} = a_u \sum_{k=1}^{N}\chi_{\hat{i},k}\sum_{k=1}^{N}\chi_{\hat{i},k}\sum_{p=1}^{\beta}c_{1,p}^2 + \sum_{p=1}^{\beta}\sum_{k=1}^{N}\chi_{\hat{i},k}a_u c_{1,p}n^{\Re}_{R,p} + \sum_{p=1}^{\beta}\sum_{k=1}^{N}\chi_{\hat{i},k}c_{1,p}n^{\Re}_{I_u,p} + \sum_{p=1}^{\beta}n^{\Re}_{R,p}n^{\Re}_{I_u,p}. \quad (19)$$

If two random variables X and Y are independent, we have $\mathrm{Var}[XY] = \mathrm{Var}[X]\mathrm{Var}[Y] + (\mathrm{E}[X])^2\mathrm{Var}[Y] + \mathrm{Var}[X](\mathrm{E}[Y])^2$, where $\mathrm{E}[\cdot]$ and $\mathrm{Var}[\cdot]$ stand for the mean and variance operators, respectively. As a consequence, the mean and variance of $D^{\Re}_{\hat{i},u}$ can be calculated as

$$\mathrm{E}[D^{\Re}_{\hat{i},u}] = a_u\frac{N^2\pi E_s}{4(1+U)} = \mu_1, \quad (20)$$

$$\mathrm{Var}[D^{\Re}_{\hat{i},u}] = (1+a_u^2)\frac{[N(4-\pi)+N^2\pi]E_sN_0}{8(1+U)} + \beta\frac{N_0^2}{4} = \sigma_1^2, \quad (21)$$

where $E_s = (1+U)\sum_{p=1}^{\beta}\mathrm{E}[c_{1,p}^2] = (1+U)\sum_{p=1}^{\beta}\mathrm{E}[c_{2,p}^2]$ is the symbol energy of RIS-JIK-MDCSK. Using the symmetry property, the mean and variance of $D^{\Im}_{\hat{i},u}$ are obtained as

$$\mathrm{E}[D^{\Im}_{\hat{i},u}] = b_u\frac{N^2\pi E_s}{4(1+U)} = \mu_2, \quad (22)$$

$$\mathrm{Var}[D^{\Im}_{\hat{i},u}] = (1+b_u^2)\frac{[N(4-\pi)+N^2\pi]E_sN_0}{8(1+U)} + \beta\frac{N_0^2}{4} = \sigma_2^2, \quad (23)$$

Since $D^{\Re}_{\hat{i},u}$ and $D^{\Im}_{\hat{i},u}$ are independent of each other, their joint probability density function (PDF) can be expressed as

$$p_{D^{\Re}_{\hat{i},u},D^{\Im}_{\hat{i},u}}(x,y) = \frac{1}{2\pi\sigma_1\sigma_2}e^{-\left[\frac{(x-\mu_1)^2}{2\sigma_1^2}+\frac{(y-\mu_2)^2}{2\sigma_2^2}\right]}. \quad (24)$$

Also, the polar coordinates transformations of $(D^{\Re}_{\hat{i},u}, D^{\Im}_{\hat{i},u})$ are introduced to ease the analysis, i.e.,

$$R = \sqrt{\left(D^{\Re}_{\hat{i},u}\right)^2 + \left(D^{\Im}_{\hat{i},u}\right)^2}, \quad (25)$$

$$\Theta = \arctan\frac{D^{\Im}_{\hat{i},u}}{D^{\Re}_{\hat{i},u}}. \quad (26)$$

Therefore, the joint PDF of R and Θ is given by

$$p_{R,\Theta}(r,\theta) = \frac{r}{2\pi\sigma_1\sigma_2}e^{-\left[\frac{(r\cos\theta-\mu_1)^2}{2\sigma_1^2}+\frac{(r\sin\theta-\mu_2)^2}{2\sigma_2^2}\right]}. \quad (27)$$

Define $\wp = \frac{(r\cos\theta-\mu_1)^2}{2\sigma_1^2} + \frac{(r\sin\theta-\mu_2)^2}{2\sigma_2^2}$. The variable $\wp$ can be further simplified as

$$\wp = \frac{\left[\sigma_2^2\cos^2\theta+\sigma_1^2\sin^2\theta\right]r^2 - 2\left[\mu_1\sigma_2^2\cos\theta+\mu_2\sigma_1^2\sin\theta\right]r}{2\sigma_1^2\sigma_2^2} + \frac{\mu_2^2\sigma_1^2+\mu_1^2\sigma_2^2}{2\sigma_1^2\sigma_2^2}$$

$$= \frac{r^2 - \frac{2\left[\mu_1\sigma_2^2\cos\theta+\mu_2\sigma_1^2\sin\theta\right]r}{\sigma_2^2\cos^2\theta+\sigma_1^2\sin^2\theta} + \frac{\mu_2^2\sigma_1^2+\mu_1^2\sigma_2^2}{\sigma_2^2\cos^2\theta+\sigma_1^2\sin^2\theta}}{\frac{2\sigma_1^2\sigma_2^2}{\sigma_2^2\cos^2\theta+\sigma_1^2\sin^2\theta}}$$

$$= \frac{\left(r - \frac{\mu_1\sigma_2^2\cos\theta+\mu_2\sigma_1^2\sin\theta}{\sigma_2^2\cos^2\theta+\sigma_1^2\sin^2\theta}\right)^2}{\frac{2\sigma_1^2\sigma_2^2}{\sigma_2^2\cos^2\theta+\sigma_1^2\sin^2\theta}}$$

$$D_{\hat{i},u} = \sum_{p=1}^{\beta}\left[\sum_{k=1}^{N}\chi_{\hat{i},k}c_{1,p} + n^{\Re}_{R,p}\right]\left[\sum_{k=1}^{N}\chi_{\hat{i},k}a_u c_{1,p} + n^{\Re}_{I_u,p}\right] + \jmath\sum_{p=1}^{\beta}\left[\sum_{k=1}^{N}\chi_{\hat{i},k}c_{2,p} + \tilde{n}^{\Re}_{R,p}\right]\left[\sum_{k=1}^{N}\chi_{\hat{i},k}b_u c_{2,p} + n^{\Im}_{I_u,p}\right], \quad (18)$$

$$+\frac{\frac{\mu_2^2\sigma_1^2+\mu_1^2\sigma_2^2}{\sigma_2^2\cos^2\theta+\sigma_1^2\sin^2\theta}-\left(\frac{\mu_1\sigma_2^2\cos\theta+\mu_2\sigma_1^2\sin\theta}{\sigma_2^2\cos^2\theta+\sigma_1^2\sin^2\theta}\right)^2}{\frac{2\sigma_1^2\sigma_2^2}{\sigma_2^2\cos^2\theta+\sigma_1^2\sin^2\theta}}$$
$$=\frac{(r-\mu_s)^2}{2\sigma_s^2}+\wp_s. \tag{28}$$

where

$$\mu_s=\frac{\mu_1\sigma_2^2\cos\theta+\mu_2\sigma_1^2\sin\theta}{\sigma_2^2\cos^2\theta+\sigma_1^2\sin^2\theta}, \tag{29}$$
$$\sigma_s^2=\frac{\sigma_1^2\sigma_2^2}{\sigma_2^2\cos^2\theta+\sigma_1^2\sin^2\theta}, \tag{30}$$
$$\wp_s=\frac{(\mu_1\sin\theta-\mu_2\cos\theta)^2}{2\left[\sigma_2^2\cos^2\theta+\sigma_1^2\sin^2\theta\right]}. \tag{31}$$

Substituting (28) into (27), the joint PDF of R and Θ can be rewritten as

$$p_{R,\Theta}(r,\theta)=\frac{r}{2\pi\sigma_1\sigma_2}e^{-\left[\frac{(r-\mu_s)^2}{2\sigma_s^2}+\wp_s\right]}$$
$$=e^{-\wp_s}\frac{r}{2\pi\sigma_1\sigma_2}e^{-\frac{(r-\mu_s)^2}{2\sigma_s^2}}. \tag{32}$$

Integrating $p_{R,\Theta}(r,\theta)$ over r, we derive the marginal PDF of θ as

$$p(\theta)=\frac{e^{-\wp_s}}{2\pi\sigma_1\sigma_2}\underbrace{\int_0^\infty re^{-\frac{(r-\mu_s)^2}{2\sigma_s^2}}\mathrm{d}r}_{\varpi_s}, \tag{33}$$

where

$$\varpi_s=\int_0^\infty re^{-\frac{(r-\mu_s)^2}{2\sigma_s^2}}\mathrm{d}r$$
$$=\int_0^\infty (r-\mu_s)e^{-\frac{(r-\mu_s)^2}{2\sigma_s^2}}\mathrm{d}r+\mu_s\int_0^\infty e^{-\frac{(r-\mu_s)^2}{2\sigma_s^2}}\mathrm{d}r$$
$$=\sigma_s^2e^{-\frac{\mu_s^2}{2\sigma_s^2}}+\sqrt{2\pi}\sigma_s\mu_sQ\left(\frac{-\mu_s}{\sigma_s}\right). \tag{34}$$

In (34), $Q(x)=\frac{1}{\sqrt{2\pi}}\int_x^{+\infty}e^{-\frac{t^2}{2}}\mathrm{d}t$ denotes the Q-function. Therefore, the PDF of θ can be obtained by putting (34) into (33). When the modulation order of the M-ary constellation is greater than 2, i.e., $M>2$, the BER of the physically modulated bits, under the condition that the events A, B, and C occur, can be computed as

$$P_{cm}\approx\frac{1}{\log_2 M}\left\{1-\int_0^{\frac{2\pi}{M}}p(\theta)\,\mathrm{d}\theta\right\}$$
$$=\frac{1}{\log_2 M}\left\{1-\frac{\varpi_s}{2\pi\sigma_1\sigma_2}\int_0^{\frac{2\pi}{M}}e^{-\wp_s}\mathrm{d}\theta\right\}. \tag{35}$$

Particularly, considering a binary constellation, i.e., $M=2$, only the in-phase component exists. The mean and variance of $D_{\hat{i},u}$ are $\mathrm{E}[D_{\hat{i},u}]=\frac{N^2\pi E_s}{4(1+U)}$ and $\mathrm{Var}[D_{\hat{i},u}]=\frac{[N(4-\pi)+N^2\pi]E_sN_0}{4(1+U)}+\beta\frac{N_0^2}{4}$, respectively. In this case, the BER of the modulated bits, under the condition that the events A, B, and C occur, is

$$P_{cm}=Q\left(\frac{\mathrm{E}[D_{\hat{i},u}]}{\sqrt{\mathrm{Var}[D_{\hat{i},u}]}}\right)$$
$$=Q\left(\sqrt{\frac{N^4\pi^2\partial^2\gamma_b^2}{4(1+U)[N(4-\pi)+N^2\pi]\partial\gamma_b+4\beta(1+U)^2}}\right), \tag{36}$$

where $\gamma_b=\frac{\gamma_s}{\partial}=\frac{E_s}{\partial N_0}$ is the bit SNR and $\gamma_s=\frac{E_s}{N_0}$ is the symbol SNR.

B. The Probability of Correct Reference Keying Detection P_A

When the signal $\mathbf{c}_1$ is transmitted as the reference signal and is erroneously detected as the signal $\mathbf{c}_4$, the reference keying detection is incorrect. To achieve correct reference keying detection, the condition $D_m>G_m$ needs to hold. Generally, there are four different cases for G_m and one case for D_m that would lead to $D_m>G_m$. The four events for G_m are $\mathcal{X}_1=A'\cap B\cap C$, $\mathcal{X}_2=A'\cap B\cap C'$, $\mathcal{X}_3=A'\cap B'\cap C$, and $\mathcal{X}_4=A'\cap B'\cap C'$, where $\cap$ denotes the intersection operation. Furthermore, $\mathcal{Y}=A\cap B\cap C$ is the event for D_m.

The decision variable corresponding to the event $\mathcal{Y}$ is

$$D_{i,u}^{\mathcal{Y}}=\sum_{p=1}^{\beta}\left[\sum_{k=1}^{N}\chi_{i,k}c_{1,p}+n_{R,p}\right]_{\Re}\left[\sum_{k=1}^{N}\chi_{i,k}c_{I_u,p}+n_{I_u,p}\right]_{\Re}$$
$$+\jmath\sum_{p=1}^{\beta}\left[\sum_{k=1}^{N}\chi_{i,k}c_{2,p}+\tilde{n}_{R,p}\right]_{\Re}\left[\sum_{k=1}^{N}\chi_{i,k}c_{I_u,p}+n_{I_u,p}\right]_{\Im}. \tag{37}$$

The means and variances of $(D_{i,u}^{\mathcal{Y}})_{\Re}$ and $(D_{i,u}^{\mathcal{Y}})_{\Im}$ are

$$\mathrm{E}[(D_{i,u}^{\mathcal{Y}})_{\Re}]=\begin{cases}\frac{N^2\pi E_s}{4(1+U)}=\mu_3, & M=2\\ a_u\frac{N^2\pi E_s}{4(1+U)}=\mu_1, & M>2\end{cases}, \tag{38}$$
$$\mathrm{E}[(D_{i,u}^{\mathcal{Y}})_{\Im}]=\begin{cases}0, & M=2\\ b_u\frac{N^2\pi E_s}{4(1+U)}=\mu_2, & M>2\end{cases}, \tag{39}$$
$$\mathrm{Var}[(D_{i,u}^{\mathcal{Y}})_{\Re}]\approx\mathrm{Var}[(D_{i,u}^{\mathcal{Y}})_{\Im}]$$
$$\approx\begin{cases}\frac{[N(4-\pi)+N^2\pi]E_sN_0}{4(1+U)}+\beta\frac{N_0^2}{4}=\sigma_3^2, & M=2\\ \frac{3[N(4-\pi)+N^2\pi]E_sN_0}{16(1+U)}+\beta\frac{N_0^2}{4}=\sigma_4^2, & M>2\end{cases}. \tag{40}$$

Furthermore, the decision variables corresponding to the events $\mathcal{X}_1$, $\mathcal{X}_2$, $\mathcal{X}_3$, and $\mathcal{X}_4$ are tabulated in Table II, where the means and variances of their real and imaginary parts are also presented.

Let A_i denote the event $D_m^{\mathcal{Y}}>G_m^{\mathcal{X}_i}, i\in\{1,2,3,4\}$, where $D_m^{\mathcal{Y}}=|D_{i,u}^{\mathcal{Y}}|$ and $G_m^{\mathcal{X}_i}=|G_{i,u}^{\mathcal{X}_i}|$, and therefore the event A is composed of four sub-events i.e., A_1, A_2, A_3, and A_4. According to the law of total probability, the probability of correct reference keying detection P_A can be formulated as

$$P_A=\frac{U}{N_RM_T}P_{A_1}+\frac{M_T-U}{N_RM_T}P_{A_2}+\frac{(N_R-1)U}{N_RM_T}P_{A_3}$$
$$+\frac{(N_R-1)(M_T-U)}{N_RM_T}P_{A_4}, \tag{41}$$

where P_{A_i} denotes the occurrence probability of the event A_i. As for the event A_1, i.e., $D_m^{\mathcal{Y}}>G_m^{\mathcal{X}_1}$, we obtain

$$P_{A_1}=\Pr\left\{D_m^{\mathcal{Y}}>G_m^{\mathcal{X}_1}\right\}=\Pr\left\{\left|D_{i,u}^{\mathcal{Y}}\right|>\left|G_{i,u}^{\mathcal{X}_1}\right|\right\}$$

TABLE II
THE DECISION VARIABLES BASED ON EVENTS $\mathcal{X}_1$, $\mathcal{X}_2$, $\mathcal{X}_3$, AND $\mathcal{X}_4$, AND THEIR MEANS AND VARIANCES

$G_{i,u}^{\mathcal{X}_1} = \sum_{p=1}^{\beta}\left[\sum_{k=1}^{N}\chi_{i,k}c_{4,p}+n_{R,p}\right]_{\Re}\left[\sum_{k=1}^{N}\chi_{i,k}c_{I_u,p}+n_{I_u,p}\right]_{\Re} + \jmath\sum_{p=1}^{\beta}\left[\sum_{k=1}^{N}\chi_{i,k}c_{5,p}+\tilde{n}_{R,p}\right]_{\Re}\left[\sum_{k=1}^{N}\chi_{i,k}c_{I_u,p}+n_{I_u,p}\right]_{\Im}$	
$\mathrm{E}[(G_{i,u}^{\mathcal{X}_1})_{\Re}] = \mathrm{E}[(G_{i,u}^{\mathcal{X}_1})_{\Im}] = 0$	$\mathrm{Var}[(G_{i,u}^{\mathcal{X}_1})_{\Re}] \approx \mathrm{Var}[(G_{i,u}^{\mathcal{X}_1})_{\Im}] \approx \begin{cases} \frac{[N(4-\pi)+N^2\pi]E_sN_0}{4(1+U)} + \beta\frac{N_0^2}{4} = \sigma_3^2, & M=2 \\ \frac{3[N(4-\pi)+N^2\pi]E_sN_0}{16(1+U)} + \beta\frac{N_0^2}{4} = \sigma_4^2, & M>2 \end{cases}$
$G_{i,u}^{\mathcal{X}_2} = \sum_{p=1}^{\beta}\left[\sum_{k=1}^{N}\chi_{i,k}c_{4,p}+n_{R,p}\right]_{\Re}\left[n_{I_u,p}\right]_{\Re} + \jmath\sum_{p=1}^{\beta}\left[\sum_{k=1}^{N}\chi_{i,k}c_{5,p}+\tilde{n}_{R,p}\right]_{\Re}\left[n_{I_u,p}\right]_{\Im}$	
$\mathrm{E}[(G_{i,u}^{\mathcal{X}_2})_{\Re}] = \mathrm{E}[(G_{i,u}^{\mathcal{X}_2})_{\Im}] = 0$	$\mathrm{Var}[(G_{i,u}^{\mathcal{X}_2})_{\Re}] = \mathrm{Var}[(G_{i,u}^{\mathcal{X}_2})_{\Im}] = \frac{[N(4-\pi)+N^2\pi]E_sN_0}{8(1+U)} + \beta\frac{N_0^2}{4} = \sigma_5^2$
$G_{i,u}^{\mathcal{X}_3} = \sum_{p=1}^{\beta}\left[\sum_{k=1}^{N}\chi_{i,k}e^{\jmath(\phi_k-\psi_{i,k})}c_{4,p}+n_{R,p}\right]_{\Re}\left[\sum_{k=1}^{N}\chi_{i,k}e^{\jmath(\phi_k-\psi_{i,k})}c_{I_u,p}+n_{I_u,p}\right]_{\Re} + \jmath\sum_{p=1}^{\beta}\left[\sum_{k=1}^{N}\chi_{i,k}e^{\jmath(\phi_k-\psi_{i,k})}c_{5,p}+\tilde{n}_{R,p}\right]_{\Re}\left[\sum_{k=1}^{N}\chi_{i,k}e^{\jmath(\phi_k-\psi_{i,k})}c_{I_u,p}+n_{I_u,p}\right]_{\Im}$	
$\mathrm{E}[(G_{i,u}^{\mathcal{X}_3})_{\Re}] = \mathrm{E}[(G_{i,u}^{\mathcal{X}_3})_{\Im}] = 0$	$\mathrm{Var}[(G_{i,u}^{\mathcal{X}_3})_{\Re}] = \mathrm{Var}[(G_{i,u}^{\mathcal{X}_3})_{\Im}] = \frac{NE_sN_0}{2(1+U)} + \beta\frac{N_0^2}{4} = \sigma_6^2$
$G_{i,u}^{\mathcal{X}_4} = \sum_{p=1}^{\beta}\left[\sum_{k=1}^{N}\chi_{i,k}e^{\jmath(\phi_k-\psi_{i,k})}c_{4,p}+n_{R,p}\right]_{\Re}\left[n_{I_u,p}\right]_{\Re} + \jmath\sum_{p=1}^{\beta}\left[\sum_{k=1}^{N}\chi_{i,k}e^{\jmath(\phi_k-\psi_{i,k})}c_{5,p}+\tilde{n}_{R,p}\right]_{\Re}\left[n_{I_u,p}\right]_{\Im}$	
$\mathrm{E}[(G_{i,u}^{\mathcal{X}_4})_{\Re}] = \mathrm{E}[(G_{i,u}^{\mathcal{X}_4})_{\Im}] = 0$	$\mathrm{Var}[(G_{i,u}^{\mathcal{X}_4})_{\Re}] = \mathrm{Var}[(G_{i,u}^{\mathcal{X}_4})_{\Im}] = \frac{NE_sN_0}{4(1+U)} + \beta\frac{N_0^2}{4} = \sigma_7^2$

$$= \int_0^{+\infty} F_{\left|G_{i,u}^{\mathcal{X}_1}\right|}(x) f_{\left|D_{i,u}^{\mathcal{Y}}\right|}(x)\,\mathrm{d}x, \tag{42}$$

where $F_{|G_{i,u}^{\mathcal{X}_1}|}(x)$ and $f_{|D_{i,u}^{\mathcal{Y}}|}(x)$ are the cumulative distribution function (CDF) of $|G_{i,u}^{\mathcal{X}_1}|$ and the PDF of $|D_{i,u}^{\mathcal{Y}}|$, respectively. Note that $(G_{i,u}^{\mathcal{X}_1})_{\Re}$, $(G_{i,u}^{\mathcal{X}_1})_{\Im}$, $(D_{i,u}^{\mathcal{Y}})_{\Re}$, and $(D_{i,u}^{\mathcal{Y}})_{\Im}$ are Gaussian random variables for a large spreading factor. Therefore, when $M = 2$, the variables $|G_{i,u}^{\mathcal{X}_1}|$ and $|D_{i,u}^{\mathcal{Y}}|$ are distributed according to the half normal distribution and folded normal distribution, respectively. Furthermore, when $M > 2$, the variables $|G_{i,u}^{\mathcal{X}_1}| = \sqrt{(G_{i,u}^{\mathcal{X}_1})_{\Re}^2 + (G_{i,u}^{\mathcal{X}_1})_{\Im}^2}$ and $|D_{i,u}^{\mathcal{Y}}| = \sqrt{(D_{i,u}^{\mathcal{Y}})_{\Re}^2 + (D_{i,u}^{\mathcal{Y}})_{\Im}^2}$ follow the Rayleigh and Rician distributions, respectively. As a result, the CDF of $|G_{i,u}^{\mathcal{X}_1}|$ and the PDF of $|D_{i,u}^{\mathcal{Y}}|$ can be expressed as (43) and (44), respectively, as shown at the bottom of the page. In (44), $\mu_0 = \sqrt{\mu_1^2 + \mu_2^2}$ and $I_0(\cdot)$ denotes the modified Bessel function of the first kind and order zero. As a consequence, the probability P_{A_1} can be obtained by putting (43) and (44) into (42). In addition, P_{A_2}, P_{A_3} and P_{A_4} can be obtained in a similar manner, and therefore the probability of correct reference keying detection P_A can eventually be obtained.

C. The Probability of Correct RIS Keying Detection P_B

The correct RIS keying detection is based on the correct reference keying detection, and therefore it is assumed that the reference signal $\mathbf{c}_1$ is detected correctly. The RIS keying modulation is intended to maximize the received SNR of the $\hat{i}$-th receive antenna. Denote $J_c = |D_{\hat{i},u}|$ and $J_r = |D_{i,u}|, i = 1, 2, \ldots, N_R - 1, i \neq \hat{i}$. Therefore, the RIS keying symbol is correctly detected when $J_c > \max(J_r)$. There are two different events for J_r, i.e., $\mathcal{Z}_1 = A \cap B' \cap C$ and $\mathcal{Z}_2 = A \cap B' \cap C'$, while one event for J_c, i.e., $\mathcal{Y} = A \cap B \cap C$. The decision variables corresponding to $\mathcal{Z}_1$ and $\mathcal{Z}_2$ are presented in Table III.

Generally, the event B can be split into two sub-events B_1 and B_2. Let $B_i, i = 1, 2$ denote the event $J_c^{\mathcal{Y}} > \max(J_r^{\mathcal{Z}_i})$, where $J_c^{\mathcal{Y}} = |D_{\hat{i},u}^{\mathcal{Y}}|$ and $J_r^{\mathcal{Z}_i} = |D_{i,u}^{\mathcal{Z}_i}|$. Note that $D_{\hat{i},u}^{\mathcal{Y}}$ is given in (37), while $D_{i,u}^{\mathcal{Z}_i}$ can be obtained from Table III. Furthermore, the probability of the event B_i is denoted by P_{B_i}. Taking the event B_1 as an example, we derive its probability as

$$\begin{aligned} P_{B_1} &= \Pr\left\{J_c^{\mathcal{Y}} > \max\left(J_r^{\mathcal{Z}_1}\right)\right\} \\ &= \Pr\left\{\left|D_{\hat{i},u}^{\mathcal{Y}}\right| > \max_{i=1,2,\ldots,N_R-1, i\neq\hat{i}}\left(\left|D_{i,u}^{\mathcal{Z}_1}\right|\right)\right\} \\ &= \int_0^{\infty}\left[F_{\left|D_{i,u}^{\mathcal{Z}_1}\right|}(x)\right]^{N_R-1} f_{\left|D_{\hat{i},u}^{\mathcal{Y}}\right|}(x)\,\mathrm{d}x, \end{aligned} \tag{45}$$

where $F_{|D_{i,u}^{\mathcal{Z}_1}|}(x) = \begin{cases} g_1(x;\sigma_6^2), M=2 \\ g_2(x;\sigma_6^2), M>2 \end{cases}$ is the CDF of $|D_{i,u}^{\mathcal{Z}_1}|$ and $f_{|D_{\hat{i},u}^{\mathcal{Y}}|}(x) = \begin{cases} g_3(x;\mu_3,\sigma_3^2), M=2 \\ g_4(x;\mu_0,\sigma_4^2), M>2 \end{cases}$ is the PDF of $|D_{\hat{i},u}^{\mathcal{Y}}|$. When

$$F_{\left|G_{i,u}^{\mathcal{X}_1}\right|}(x) = \begin{cases} \mathrm{erf}\left(\frac{x}{\sqrt{2\sigma_3^2}}\right) = g_1\left(x;\sigma_3^2\right), \; M = 2 \\ 1 - e^{-\frac{x^2}{2\sigma_4^2}} = g_2\left(x;\sigma_4^2\right), \quad M > 2 \end{cases}, \tag{43}$$

$$f_{\left|D_{i,u}^{\mathcal{Y}}\right|}(x) = \begin{cases} \frac{1}{\sqrt{2\pi\sigma_3^2}}\left[e^{-\frac{(x-\mu_3)^2}{2\sigma_3^2}} + e^{-\frac{(x+\mu_3)^2}{2\sigma_3^2}}\right] = g_3\left(x;\mu_3,\sigma_3^2\right), \; M = 2 \\ \frac{x}{\sigma_4^2}e^{-\frac{x^2+\mu_0^2}{2\sigma_4^2}} I_0\left(\frac{x\mu_0}{\sigma_4^2}\right) = g_4\left(x;\mu_0,\sigma_4^2\right), \qquad M > 2 \end{cases}, \tag{44}$$

TABLE III
THE DECISION VARIABLES BASED ON THE EVENTS $\mathcal{Z}_1$ AND $\mathcal{Z}_2$, AND THEIR MEANS AND VARIANCES

$D_{i,u}^{\mathcal{Z}_1}=\sum_{p=1}^{\beta}\left[\sum_{k=1}^{N}\chi_{i,k}e^{\jmath(\phi_k-\psi_{i,k})}c_{1,p}+n_{R,p}\right]_{\Re}\left[\sum_{k=1}^{N}\chi_{i,k}e^{\jmath(\phi_k-\psi_{i,k})}c_{I_u,p}+n_{I_u,p}\right]_{\Re} +\jmath\sum_{p=1}^{\beta}\left(\sum_{k=1}^{N}\chi_{i,k}e^{\jmath(\phi_k-\psi_{i,k})}c_{2,p}+\tilde{n}_{R,p}\right)_{\Re}\left(\sum_{k=1}^{N}\chi_{i,k}e^{\jmath(\phi_k-\psi_{i,k})}c_{I_u,p}+n_{I_u,p}\right)_{\Im}$	
$\mathrm{E}[(D_{i,u}^{\mathcal{Z}_1})_{\Re}]=\mathrm{E}[(D_{i,u}^{\mathcal{Z}_1})_{\Im}]=0$	$\mathrm{Var}[(D_{i,u}^{\mathcal{Z}_1})_{\Re}]=\mathrm{Var}[(D_{i,u}^{\mathcal{Z}_1})_{\Im}]=\frac{NE_sN_0}{2(1+U)}+\beta\frac{N_0^2}{4}=\sigma_6^2$
$D_{i,u}^{\mathcal{Z}_2}=\sum_{p=1}^{\beta}\left[\sum_{k=1}^{N}\chi_{i,k}e^{\jmath(\phi_k-\psi_{i,k})}c_{1,p}+n_{R,p}\right]_{\Re}\left[n_{I_u,p}\right]_{\Re}+\jmath\sum_{p=1}^{\beta}\left[\sum_{k=1}^{N}\chi_{i,k}e^{\jmath(\phi_k-\psi_{i,k})}c_{2,p}+\tilde{n}_{R,p}\right]_{\Re}\left[n_{I_u,p}\right]_{\Im}$	
$\mathrm{E}[(D_{i,u}^{\mathcal{Z}_2})_{\Re}]=\mathrm{E}[(D_{i,u}^{\mathcal{Z}_2})_{\Im}]=0$	$\mathrm{Var}[(D_{i,u}^{\mathcal{Z}_2})_{\Re}]=\mathrm{Var}[(D_{i,u}^{\mathcal{Z}_2})_{\Im}]=\frac{NE_sN_0}{4(1+U)}+\beta\frac{N_0^2}{4}=\sigma_7^2$

σ_6^2 in $F_{|D_{i,u}^{\mathcal{Z}_1}|}(x)$ is replaced by σ_7^2 given in Table III, the probability of the event B_2 can be obtained. Therefore, the occurrence probability of the event B is given by

$$P_B=\frac{U}{M_T}P_{B_1}+\frac{M_T-U}{M_T}P_{B_2}. \tag{46}$$

D. The Probability of Correct Carrier Keying Detection P_C

Define the index of the activated carrier as v. Assuming correct reference keying detection and correct RIS keying detection, when the activated carriers are correctly detected, the corresponding decision variable, denoted by $D_{i,v}^c, v=1,2,\ldots,U$, is the same as that in (37). In addition, when the receiver detects the inactivated carriers ($u\neq v$), the decision variable $D_{i,u}^e, u=1,2,\ldots,M_T-U, u\neq v$ is given by

$$D_{i,u}^e=\sum_{p=1}^{\beta}\left[\sum_{k=1}^{N}\chi_{i,k}c_{1,p}+n_{R,p}\right]_{\Re}[n_{I_u,p}]_{\Re} +\jmath\sum_{p=1}^{\beta}\left[\sum_{k=1}^{N}\chi_{i,k}c_{2,p}+\tilde{n}_{R,p}\right]_{\Re}[n_{I_u,p}]_{\Im}, \tag{47}$$

with $\mathrm{E}[(D_{i,u}^e)_{\Re}]=\mathrm{E}[(D_{i,u}^e)_{\Im}]=0$ and $\mathrm{Var}[(D_{i,u}^e)_{\Re}]=\mathrm{Var}[(D_{i,u}^e)_{\Im}]=\frac{[N(4-\pi)+N^2\pi]E_sN_0}{4(1+U)}+\beta\frac{N_0^2}{4}=\sigma_3^2$. Also, when the minimum value of $|D_{i,v}^c|$ is greater than the maximum value of $|D_{i,u}^e|$, the activated carriers can be correctly detected. Therefore, the probability of correct carrier keying detection can be formulated as

$$\begin{aligned}P_C&=\Pr\left\{\min_{v=1,2,\ldots,U}\left(|D_{i,v}^c|\right)>\max_{u=1,2,\ldots,M_T-U,u\neq v}\left(|D_{i,u}^e|\right)\right\}\\&=\int_0^{\infty}F_{|D_{i,u}^e|}^{M_T-U}(x)U\left[1-F_{|D_{i,v}^c|}(x)\right]^{U-1}f_{|D_{i,v}^c|}(x)\mathrm{d}x,\end{aligned} \tag{48}$$

where $F_{|D_{i,u}^e|}(x)=\begin{cases}g_1(x;\sigma_3^2),M=2\\g_2(x;\sigma_3^2),M>2\end{cases}$ denotes the CDF of $|D_{i,u}^e|$. In addition, $f_{|D_{i,v}^c|}(x)$ is the PDF of $|D_{i,v}^c|$, given by $f_{|D_{i,v}^c|}(x)=\begin{cases}g_3(x;\mu_3,\sigma_3^2),M=2\\g_4(x;\mu_0,\sigma_4^2),M>2\end{cases}$, and $F_{|D_{i,v}^c|}(x)$ is the CDF of $|D_{i,v}^c|$, given by

$$F_{|D_{i,v}^c|}(x)=\begin{cases}\frac{1}{2}\left[\mathrm{erf}\left(\frac{x+\mu_1}{\sqrt{2\sigma_3^2}}\right)+\mathrm{erf}\left(\frac{x-\mu_1}{\sqrt{2\sigma_3^2}}\right)\right], & M=2\\ 1-Q_1\left(\frac{\mu_0}{\sigma_4},\frac{x}{\sigma_4}\right), & M>2\end{cases}, \tag{49}$$

where $Q_1(\cdot,\cdot)$ is the Marcum Q-function.

E. The Overall BER of the RIS-JIK-MDCSK System

The total information bits transmitted by an RIS-JIK-MDCSK symbol include one reference keying bit, n_c RIS keying bits, m_c carrier keying bits, and Un physically modulated bits. Therefore, the overall bit error probability of RIS-JIK-MDCSK is determined by the BERs of the reference keying bit, RIS keying bits, carrier keying bits, and physically modulated bits, denoted by P_{J_1}, P_{J_2}, P_{J_3}, and P_{J_4}, respectively. Therefore, the BER of the RIS-JIK-MDCSK system can be derived according to the law of total probability, yielding

$$P_J=\frac{1}{\partial}P_{J_1}+\frac{n_c}{\partial}P_{J_2}+\frac{m_c}{\partial}P_{J_3}+\frac{Un}{\partial}P_{J_4}. \tag{50}$$

Since only one reference keying bit is transmitted, the BER of the reference keying bit is equal to the error probability of the reference keying detection, i.e.,

$$P_{J_1}=P_{A'}. \tag{51}$$

In addition, the BER of the RIS keying bits can be formulated as

$$P_{J_2}=P_A\frac{2^{n_c-1}}{2^{n_c}-1}P_{B'}+\frac{1}{2}P_{A'}, \tag{52}$$

where the first summand on the right side corresponds the case that the reference keying detection is correct but the RIS keying bits are erroneously recovered with error probability $\frac{2^{n_c-1}}{2^{n_c}-1}P_{B'}$, while the second summand corresponds to the error probability that the RIS keying bits are estimated based on the incorrect reference keying detection. Similarly, the BER of the carrier keying bits can be expressed as

$$P_{J_3}=P_AP_B\eta P_{C'}+\frac{1}{2}P_AP_{B'}+\frac{1}{2}P_{A'}, \tag{53}$$

where the coefficient η gives the relationship between the error probabilities of carrier keying detection and the BER of carrier keying bits, given by [25]

$$\eta=\frac{2^{m_c-1}\left[2C_{M_T}^U-2^{m_c}\right]}{C_{M_T}^U[C_{M_T}^U-1]}. \tag{54}$$

The BER of the physically modulated bits is obtained as

$$P_{J_4}=P_AP_BP_CP_{cm}+\frac{1}{2}P_AP_BP_{C'}+\frac{1}{2}P_AP_{B'}+\frac{1}{2}P_{A'}. \tag{55}$$

Finally, the total bit error probability of the proposed RIS-JIK-MDCSK system can be obtained by substituting (51), (52), (53), and (55) into (50). According to (51)–(55), we can conclude that the BER of the reference keying bit P_{J_1} has the greatest impact on the BER performance of RIS-JIK-MDCSK, because P_{J_2}, P_{J_3}, and P_{J_4} depend on $P_{A'}$, where $P_{A'} = P_{J_1}$. In other words, the reference keying detection has the greatest effect on the BER performance of RIS-JIK-MDCSK.

IV. Throughput, Spectral Efficiency, and System Complexity Analysis

A. Throughput and Spectral Efficiency Analysis

In this subsection, the throughput and spectral efficiency are analyzed to verify the advantages of the proposed RIS-JIK-MDCSK system. Furthermore, we compare the throughput and spectral efficiency of the proposed system with other systems.

Generally, the throughput refers to the ratio of the number of correctly recovered symbols to the required transmission time [51], [52]. In RIS-JIK-MDCSK, ∂ information bits are transmitted in a symbol, and the symbol is correctly retrieved if and only if all ∂ bits are correctly recovered. Therefore, the throughput of the proposed RIS-JIK-MDCSK system can be formulated as

$$\Omega_1 = \frac{N_{sym}\left(1 - P_J\right)^{\partial}}{\left(1 + M_T\right)\beta T_c} \quad \text{[symbols/sec]}, \tag{56}$$

where N_{sym} is the number of transmitted symbols and T_c is the chip duration of the chaotic sequence. Furthermore, it is assumed that the RIS-JIK-MDCSK system and the other systems have the same numbers of subcarriers and transmitted symbols. According to the definition of throughput, the throughputs of MC-DCSK [26], GCI-DCSK [35], CI-MDCSK [36], and CIM-MC-MDCSK [37] systems are $\Omega_2 = \frac{N_{sym}(1-P_{MC})^{M_T}}{(1+M_T)\beta T_c}$, $\Omega_3 = \frac{N_{sym}(1-P_{GCI})^{\lfloor \log_2 C_{M_T}^U \rfloor + U}}{(1+M_T)\beta T_c}$, $\Omega_4 = \frac{N_{sym}(1-P_{CI})^{\lfloor \log_2 M_T \rfloor + n}}{(1+M_T)\beta T_c}$, and $\Omega_5 = \frac{N_{sym}(1-P_{CIM})^{\lfloor \log_2 N_w \rfloor + n N_w}}{N_w \beta T_c}$, respectively, where P_{MC}, P_{GCI}, P_{CI}, and P_{CIM} denote the BERs of MC-DCSK, GCI-DCSK, CI-MDCSK, and CIM-MC-MDCSK, respectively. In addition, N_w denotes the length of the Walsh codes in the CIM-MC-MDCSK system.

The spectral efficiency is defined as the ratio of the total data rate to the required bandwidth [53], [54], which provides the number of bits per second that can be transmitted in a given bandwidth. It is assumed that the bandwidth of each subcarrier is B_w. The RIS-JIK-MDCSK system is capable of transmitting ∂ information bits in a symbol duration, and therefore the spectral efficiency is obtained as

$$\Psi_1 = \frac{\text{bit rate}}{\text{total bandwidth}} = \frac{\frac{\partial}{\beta T_c}}{\left(1 + M_T\right) B_w} \quad \text{[bits/sec/Hz]}. \tag{57}$$

In addition, the spectral efficiencies of the MC-DCSK [26], GCI-DCSK [35], CI-MDCSK [36], and CIM-MC-MDCSK [37] systems can be calculated as $\Psi_2 = \frac{M_T}{(1+M_T)\beta T_c B_w}$, $\Psi_3 = \frac{\lfloor \log_2 C_{M_T}^U \rfloor + U}{(1+M_T)\beta T_c B_w}$, $\Psi_4 = \frac{\lfloor \log_2 M_T \rfloor + n}{(1+M_T)\beta T_c B_w}$, and $\Psi_5 = \frac{\lfloor \log_2 N_w \rfloor + n N_w}{N_w \beta T_c B_w}$, respectively.

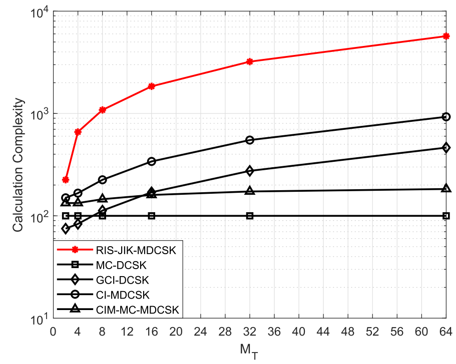

Fig. 4. Computational complexity of the proposed RIS-JIK-MDCSK, MC-DCSK [26], GCI-DCSK [35], CI-MDCSK [36], and CIM-MC-MDCSK [37] systems.

B. Analysis and Comparison of System Complexity

In this subsection, the system complexity of the proposed RIS-JIK-MDCSK system is analyzed and compared to that of the considered benchmark systems. At the RIS-JIK-MDCSK transmitter, U out of M_T subcarriers are activated to transmit the M-ary information-bearing signals, and the remaining $M_T - U$ subcarriers are inactivated. Furthermore, each M-ary information-bearing signal requires 2β spreading operations. Consequently, the number of multiplications used at the RIS-JIK-MDCSK transmitter is $2\beta U$. As shown in the proposed joint index keying detection algorithm, the RIS-JIK-MDCSK receiver needs $4\beta N_R M_T$ multiplications to retrieve all information bits. The number of multiplications required for the transmission of one bit can be used to evaluate the computational complexity. Therefore, the total computational complexity of the proposed RIS-JIK-MDCSK system is given by

$$\begin{aligned}\mathcal{O}_1 =& \frac{2\beta U + 4\beta N_R M_T}{1 + n_c + m_c + Un} \\ =& \frac{2\beta\left(U + 2N_R M_T\right)}{1 + \lfloor \log_2 N_R \rfloor + \lfloor \log_2 C_{M_T}^U \rfloor + Un}.\end{aligned} \tag{58}$$

Similarly, the computational complexities of MC-DCSK [26], GCI-DCSK [35], CI-MDCSK [36], and CIM-MC-MDCSK [37] can be obtained as $\mathcal{O}_2 = \frac{2\beta M_T}{M_T}$, $\mathcal{O}_3 = \frac{\beta(U+M_T)}{\lfloor \log_2 C_{M_T}^U \rfloor + U}$, $\mathcal{O}_4 = \frac{2\beta(1+M_T)}{\lfloor \log_2 M_T \rfloor + n}$, and $\mathcal{O}_5 = \frac{4\beta N_w}{\lfloor \log_2 N_w \rfloor + n N_w}$, respectively. As shown in Fig. 4, we compare the computational complexity of RIS-JIK-MDCSK with that of the benchmark systems by assuming $U = 1$, $\beta = 50$, $N_R = 2$, and $N_w = M_T$. As can be seen from Fig. 4, the computational complexity of RIS-JIK-MDCSK is higher than that of the benchmark systems. In addition, the hardware complexity comparison between the proposed RIS-JIK-MDCSK and other DCSK-based systems is shown in Table IV. RIS-JIK-MDCSK has a higher hardware complexity than the other systems, since three Hilbert filters are used in the muti-stream chaotic generator, and one Hilbert filter and N_R receive antennas are used at the RIS-JIK-MDCSK receiver. Therefore, the system complexity of RIS-JIK-MDCSK, including the computational and hardware complexities, is higher than the benchmark systems.

TABLE IV

HARDWARE COMPLEXITY COMPARISON BETWEEN THE PROPOSED RIS-JIK-MDCSK AND BENCHMARK SYSTEMS

Systems	Hilbert filters	Shaping filters	Matched filters	Receive antennas	Other blocks
Proposed RIS-JIK-MDCSK	4	$U+1$	M_T+1	N_R	Reference keying, RIS controller, RIS
MC-DCSK [26]	0	M_T+1	M_T+1	1	——
GCI-DCSK [35]	0	$U+1$	M_T+1	1	——
CI-MDCSK [36]	2	2	M_T+1	1	——
CIM-MC-MDCSK [37]	2	$2M_T$	$2M_T$	1	Walsh code generator, Walsh code synchronizer

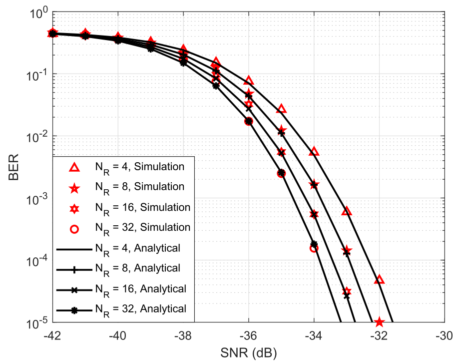

Fig. 5. BER of RIS-JIK-MDCSK as a function of N_R over Rayleigh fading channels.

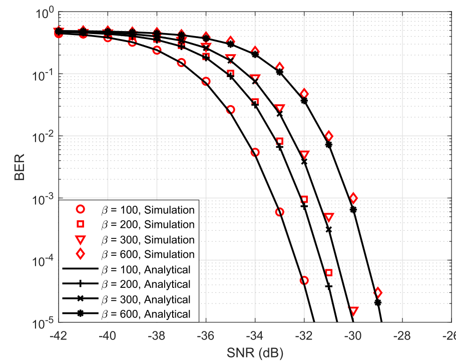

Fig. 6. BER of RIS-JIK-MDCSK as a function of β over Rayleigh fading channels.

However, in Section V, we will demonstrate that the proposed RIS-JIK-MDCSK system outperforms the benchmark systems in terms of throughput, spectral efficiency, and BER.

V. NUMERICAL RESULTS AND DISCUSSIONS

In this section, we carry out computer simulations to evaluate the performance of the proposed RIS-JIK-MDCSK system. The analytical results obtained by using the analytical expressions of the BER are also presented to verify the correctness of the performance analysis. First, we evaluate the impact of different system parameters on the BER of the proposed RIS-JIK-MDCSK system. Second, the throughput and spectral efficiency of RIS-JIK-MDCSK are compared against the benchmarks. Finally, the BER of the proposed RIS-JIK-MDCSK system is compared with other RIS-aided systems and non-coherent DCSK-based systems to obtain some insightful findings.

A. Impact of Different System Parameters on the BER of RIS-JIK-MDCSK

In Fig. 5, we study the BER of the proposed RIS-JIK-MDCSK system with respect to the number of receive antennas N_R over Rayleigh fading channels. The simulation parameters are $N = 200$, $M_T = 4$, $U = 2$, $\beta = 100$, and $M = 2$. The performance gap between $N_R = 32$ and $N_R = 4$ is more than 1.5 dB at BER $= 10^{-5}$. The analytical BER is in good agreement with the simulated BER, which verifies the correctness of the performance analysis in Section III.

The BER of RIS-JIK-MDCSK as a function of the spreading factors β is investigated in Fig. 6. The system parameters are $N = 200$, $M_T = 4$, $U = 2$, $N_R = 4$, and $M = 2$. By increasing β, we see that the proposed RIS-JIK-MDCSK system suffers from some performance degradation. For example, when BER $= 10^{-5}$, the proposed RIS-JIK-MDCSK system with $\beta = 100$ can achieve more than 3 dB performance gain compared to that of $\beta = 600$ because the noise term in (18) becomes more important for large β.

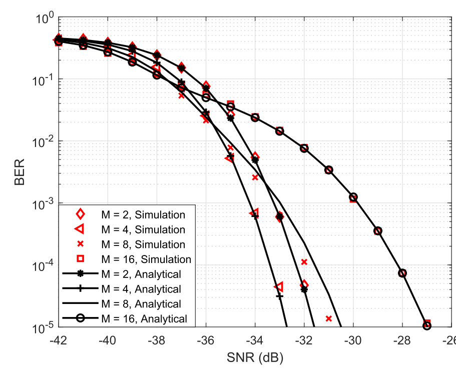

Fig. 7. BER of RIS-JIK-MDCSK as a function of M over Rayleigh fading channels.

Fig. 7 shows the BER of RIS-JIK-MDCSK for different modulation orders M over Rayleigh fading channels. The system parameters are $N_R = 4$, $M_T = 4$, $U = 2$, $\beta = 100$, and $N = 200$. RIS-JIK-MDCSK with $M = 4$ achieves the best BER. When M is increased from 4 to 16, however, the proposed RIS-JIK-MDCSK system has a declining BER performance, because the distance between the adjacent constellation points is reduced, thereby leading to a large error probability for the MDCSK demodulation. The simulation results for $M = 8$ have a slight disagreement with the theoretical estimates, because P_{cm} in (35), $\mathrm{Var}[(D_{i,u}^{\mathcal{Y}})_{\Re}]$ and $\mathrm{Var}[(D_{i,u}^{\mathcal{Y}})_{\Im}]$ in (40), and $\mathrm{Var}[(G_{i,u}^{\mathcal{X}_1})_{\Re}]$ and $\mathrm{Var}[(G_{i,u}^{\mathcal{X}_1})_{\Im}]$ in Table II are approximated results.

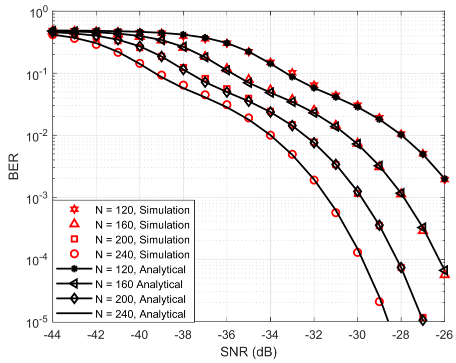

Fig. 8. BER of RIS-JIK-MDCSK as a function of N over Rayleigh fading channels.

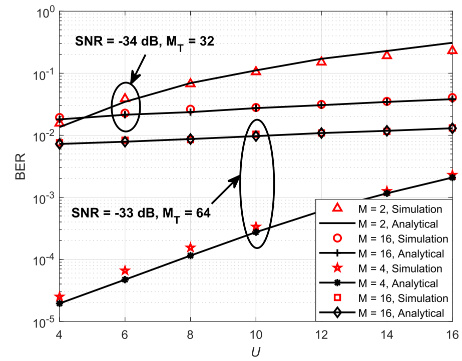

Fig. 10. The impact of U on the BER of RIS-JIK-MDCSK over Rayleigh fading channels.

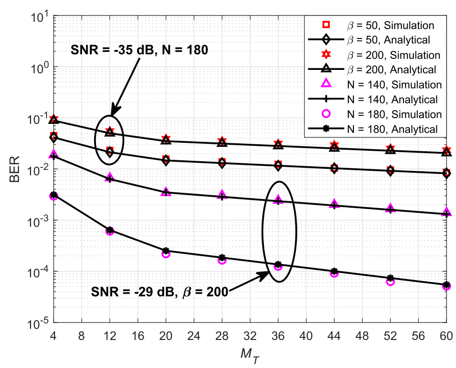

Fig. 9. The impact of M_T on the BER of RIS-JIK-MDCSK over Rayleigh fading channels.

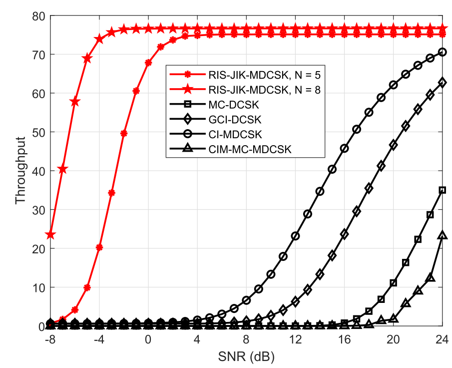

Fig. 11. Throughput comparison between the proposed RIS-JIK-MDCSK, MC-DCSK [26], GCI-DCSK [35], CI-MDCSK [36], and CIM-MC-MDCSK [37] systems.

As shown in Fig. 7, the curve for $M = 16$ crosses that for $M = 8$. This phenomenon can be explained as follows. The BER of the reference keying bit and the RIS keying bits for $M = 16$ is lower than that for $M = 8$. This is because for a given SNR and given energy of the transmitted signal, more information bits can be transmitted by RIS-JIK-MDCSK when M is increased from 8 to 16, which reduces the variance of the noise and therefore decreases the BER of the reference keying bit and the RIS keying bits. When $-42\text{dB} < \text{SNR} < -38\text{dB}$, the BER of RIS-JIK-MDCSK mainly depends on the BER of the reference keying bit and the RIS keying bits. Therefore, RIS-JIK-MDCSK with $M = 16$ outperforms that with $M = 8$ if $-42\text{dB} < \text{SNR} < -38\text{dB}$. However, when the SNR increases, i.e., $\text{SNR} > -38\text{dB}$, the BER of the physically modulated bits becomes the dominant part of the BER of RIS-JIK-MDCSK. When M increases from 8 to 16, the BER of the physically modulated bits increases rapidly, because the distance between adjacent constellation symbols is decreased. Therefore, when $\text{SNR} > -38\text{dB}$, the BER of RIS-JIK-MDCSK for $M = 16$ is higher than that for $M = 8$. Therefore, it is concluded that the curve for $M = 16$ crosses that for $M = 8$. The reason why the curves for $M = 8$ and $M = 16$ cross the counterparts for $M = 2$ and $M = 4$ is similar.

The simulated and analytical BER of RIS-JIK-MDCSK as a function of the numbers of RIS elements N over Rayleigh fading channels are plotted in Fig. 8. The system parameters are $U = 2$, $N_R = 4$, $M_T = 4$, $M = 16$, and $\beta = 100$. The simulation results well match the corresponding analytical results. In addition, when N is increased from 120 to 240, the BER of RIS-JIK-MDCSK is decreased. For example, at $\text{BER} = 10^{-5}$, RIS-JIK-MDCSK with $N = 240$ outperforms that with $N = 200$ and $N = 160$ by about 1.5 dB and 3.5 dB, respectively.

Fig. 9 shows the impact of the number of information-bearing subcarriers M_T on the BER of RIS-JIK-MDCSK over Rayleigh fading channels. The system parameters are $M = 16$, $N_R = 4$, and $U = 3$. As observed from Fig. 9, the BER of the RIS-JIK-MDCSK system is decreases with the increase of M_T, because more carrier keying bits are transmitted and the required SNR to achieve a specific BER is reduced. Therefore, the parameter M_T can be set as large as possible to obtain superior BER performance. In addition, RIS-JIK-MDCSK can achieve better performance by increasing N and decreasing β, which is consistent with the observations in Figs. 6 and 8.

In Fig. 10, the impact of the number of activated information-bearing subcarriers U on the BER performance of the proposed RIS-JIK-MDCSK system is investigated. The simulation parameters are $N = 160$, $N_R = 4$, and $\beta = 100$. As shown in Fig. 10, the simulated BER curves are in agreement with the analytical ones. Furthermore, the BER of the proposed RIS-JIK-MDCSK system gets worse when increasing U, because the inter-symbol interference increases for large values of U. Therefore, we can configure RIS-JIK-MDCSK with a small U to obtain better BER performance.

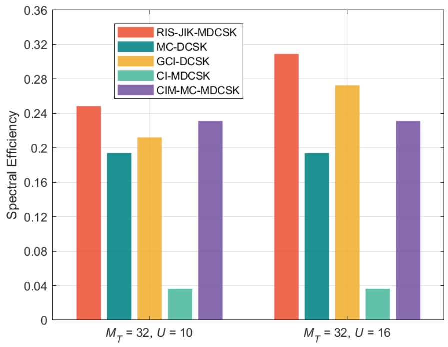

Fig. 12. Spectral efficiency comparison between the proposed RIS-JIK-MDCSK, MC-DCSK [26], GCI-DCSK [35], CI-MDCSK [36], and CIM-MC-MDCSK [37] systems.

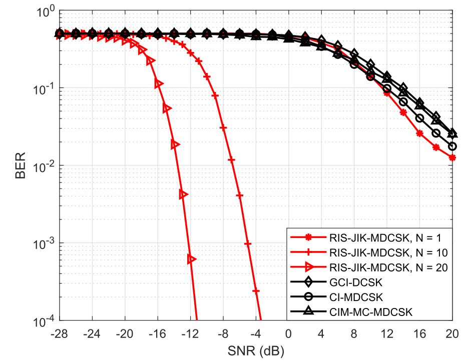

Fig. 13. BER comparison between the proposed RIS-JIK-MDCSK system and other systems assuming the same number of subcarriers.

Remark 2: As shown in Figs. 5–10, when the modulation order is $M = 4$, the proposed RIS-JIK-MDCSK system exhibits better BER performance. Furthermore, large values of N_R, N, and M_T contribute to the enhancement of the BER performance of RIS-JIK-MDCSK, while small values of β and U enable RIS-JIK-MDCSK to achieve better BER performance. However, when the parameters N_R, N, and M_T increase, the complexity of RIS-JIK-MDCSK also increases. Therefore, there is a trade off between BER performance and system complexity.

B. Throughput and Spectral Efficiency of RIS-JIK-MDCSK Compared to Other DCSK-Based Systems

In this subsection, the throughput and spectral efficiency of the proposed RIS-JIK-MDCSK system are compared against other DCSK-based systems. The following systems are considered for benchmarking: MC-DCSK [26], GCI-DCSK [35], CI-MDCSK [36], and CIM-MC-MDCSK [37].

In Fig. 11, we compare the throughput of RIS-JIK-MDCSK against the benchmark systems, based on the analysis in Subsection IV-A. The system parameters are $\beta = 200$, $T_c = 10$ μs, $N_{sym} = 10$, $M_T = 64$, and $M = 2$. Furthermore, $N_R = 2$ and $U = 1$ are assumed for RIS-JIK-MDCSK. In CI-MDCSK, one of the 64 information-bearing subcarriers is activated. In addition, half of information-bearing subcarriers are activated in GCI-DCSK. The length of the Walsh codes in CIM-MC-MDCSK is $N_w = 64$. As can be seen from Fig. 11, the proposed RIS-JIK-MDCSK system equipped with 5 RIS elements can achieve high a throughput when the SNR is lower than 0 dB. With the increase of SNR, the throughput of the proposed RIS-JIK-MDCSK system outperforms the other DCSK-based systems. This is due to the low BER of RIS-JIK-MDCSK, leading to a large number of correctly recovered symbols, i.e., large value of $N_{sym}(1 - P_J)^{\partial}$ in (56), for a given N_{sym}. This, in turn, contributes to the high throughput of RIS-JIK-MDCSK.

The spectral efficiency comparison between the RIS-JIK-MDCSK, MC-DCSK, CI-MDCSK, GCI-DCSK, and CIM-MC-MDCSK systems is shown in Fig. 12, where $T_c B_w = 0.05$, $\beta = 100$, and $M = 2$ are assumed. In addition, $N_R = 32$ is considered for RIS-JIK-MDCSK. The length of the Walsh codes N_w used for the CIM-MC-MDCSK system is $N_w = 32$. In Fig. 12, it is clearly observed that the proposed RIS-JIK-MDCSK system provides the highest spectral efficiency compared to the benchmark systems. The main reason is that RIS-JIK-MDCSK capitalizes on the benefits of the joint keying, i.e., additional information bits are implicitly transmitted by the indices of the reference keying, RIS keying, and carrier keying.

C. BER Comparison Between the Proposed RIS-JIK-MDCSK System and the Benchmark Systems

In this subsection, we compare the BER of the proposed RIS-JIK-MDCSK system, DCSK-based systems, and RIS-aided index modulation systems. The benchmark systems include RIS-SM [9], RIS-SSK [9], MC-DCSK [26], GCI-DCSK [35], CI-MDCSK [36], and CIM-MC-MDCSK [37] systems.

Fig. 13 compares the BER of the proposed RIS-JIK-MDCSK system and the DCSK-based systems, where the number of subcarriers is identical and equal to 33. In addition, the spreading factor $\beta = 50$ is used in all systems and the modulation order for all MDCSK variants is $M = 2$. The simulation parameters are as follows: $N_R = 2$, $M_T = 32$, and $U = 16$ are applied in RIS-JIK-MDCSK, the number of activated subcarriers in GCI-DCSK is the same as in RIS-JIK-MDCSK. As shown in Fig. 13, the proposed RIS-JIK-MDCSK system equipped with one-element RIS is capable of obtaining better BER performance compared to other systems. When the number of RIS elements is increased to $N = 10$, the RIS-JIK-MDCSK system outperforms CI-MDCSK by more than 20 dB at the BER level of 10^{-2}. The BER performance gain offered by RIS-JIK-MDCSK can be further expanded by increasing the number of RIS elements.

As shown in Fig. 14, the BER of the proposed RIS-JIK-MDCSK system is compared to that of other systems for the same number of transmitted bits, i.e., $\partial = 24$ and $\partial = 36$. Furthermore, all systems have the same spreading factor $\beta = 100$. When $\partial = 24$, the parameters $M_T = 22$ and $U = 6$ are used in RIS-JIK-MDCSK, while $M_T = 25$ and $U = 12$ are used when $\partial = 36$. Other parameters of RIS-JIK-MDCSK are $N_R = 2$ and $M = 2$. Moreover, in GCI-DCSK, 8 out of 20 information-bearing subcarriers are activated to transmit the modulated bits. For the CIM-MC-MDCSK system, the length

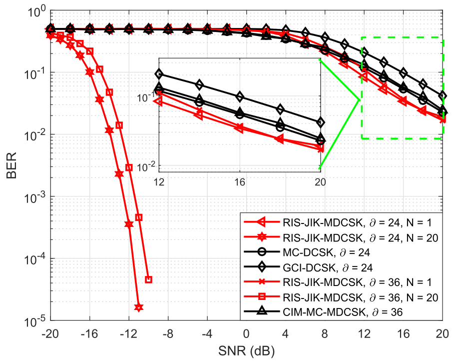

Fig. 14. BER comparison between the proposed RIS-JIK-MDCSK system and other systems assuming the same number of transmitted bits.

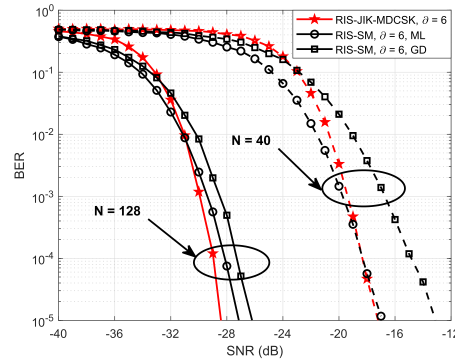

Fig. 16. BER of the proposed RIS-JIK-MDCSK and RIS-SM [9] systems assuming the same number of transmitted bits.

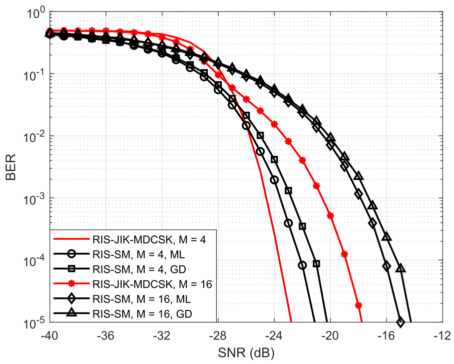

Fig. 15. BER of the proposed RIS-JIK-MDCSK and RIS-SM [9] systems assuming the same number of receive antennas.

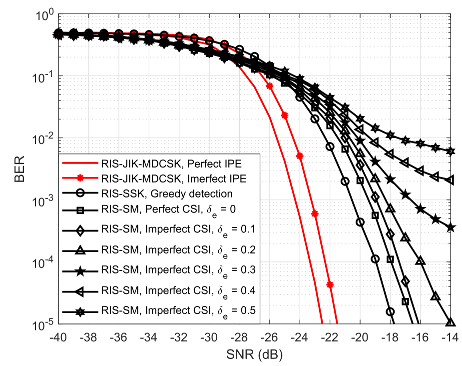

Fig. 17. BER comparison between the proposed RIS-JIK-MDCSK, RIS-SSK [9], and RIS-SM [9] systems.

of the Walsh codes and the modulation order of the M-ary constellation are 16 and 4, respectively. It is apparent that the proposed RIS-JIK-MDCSK system outperforms the other DCSK-based systems for different ∂. Even for $N = 1$, the performance gain achieved by RIS-JIK-MDCSK is better than the other systems by about 2 dB. With a large N, the proposed RIS-JIK-MDCSK system can obtain a higher performance gain.

As shown in Figs. 13 and 14, the proposed RIS-JIK-MDCSK system can achieve a significant BER performance gain by increasing the number of RIS elements. The main reason is that according to (20)–(23) and (36), a large value of N leads to a large value of $\frac{\mathrm{E}[D_{\hat{i},u}]}{\sqrt{\mathrm{Var}[D_{\hat{i},u}]}}$. The Q-function is a monotonically decreasing function. According to (36), when N increases, the error probability P_{cm} decreases, leading to a low BER for RIS-JIK-MDCSK. There are two reasons why the proposed RIS-JIK-MDCSK system outperforms the other DCSK-based systems. On the one hand, the proposed RIS-JIK-MDCSK system is capable of adjusting the phases of RIS elements to maximize the received SNR for the desired receive antenna, therefore improving the BER. On the other hand, the joint keying mechanism is exploited in RIS-JIK-MDCSK to enhance the BER.

In Fig. 15, the BER of RIS-JIK-MDCSK is compared to that of RIS-SM, where ML and GD denote the maximum likelihood detection and greedy detection, respectively. The system parameters are $M_T = 8$, $U = 2$, and $\beta = 100$. Moreover, the number of RIS elements and receive antennas for all systems is identical and equal to $N = 64$ and $N_R = 4$, respectively. As observed in Fig. 15, considering the BER level of 10^{-5} and $M = 4$, the proposed RIS-JIK-MDCSK system can offer about 2 dB and 3 dB performance gain compared to RIS-SM equipped with ML and GD, respectively. When M is increased to 16, the corresponding gain increases to 3 dB and 4 dB, respectively.

The BER of the RIS-JIK-MDCSK and RIS-SM systems assuming the same number of transmitted bits, i.e., $\partial = 6$, is studied in Fig. 16. Both RIS-JIK-MDCSK and RIS-SM possess an identical number of RIS elements and modulation order, i.e., $N = 128, 40$ and $M = 4$. When $N = 40$, RIS-SM with the ML detector can achieve similar BER performance as RIS-JIK-MDCSK at $\mathrm{BER} = 10^{-5}$. However, RIS-SM with GD suffers from about 3 dB loss in BER performance. When N is increased to 128, the proposed RIS-JIK-MDCSK system outperforms RIS-SM with both ML and GD by about 1 dB and 2 dB, respectively. The improved BER performance of the proposed RIS-JIK-MDCSK system over the RIS-SM system is due to the utilization of all three keying mechanisms, including reference keying, RIS keying, and carrier keying, in the RIS-JIK-MDCSK system, whereas only RIS keying is utilized in the RIS-SM system.

As shown in Fig. 17, we compare the BER of the proposed RIS-JIK-MDCSK with perfect and imperfect initial phase estimation (IPE), RIS-SSK with greedy detection, and RIS-SM with imperfect CSI. The number of RIS elements is $N = 64$ and the number of transmitted bits per symbol is $\partial = 7$ for all systems. Furthermore, $N_R = 4$, $M_T = 4$, $U = 1$, $M = 4$, and $\beta = 100$ are assumed for RIS-JIK-MDCSK. $N_R = 128$ is considered for RIS-SSK. $N_R = 16$ and $M = 8$ are set for RIS-SM. When imperfect CSI is used for RIS-SM, the estimated channel for RIS-SM is given by $\hat{g}_{i,k}^{est} = \hat{g}_{i,k} + n_{i,k}$, where $\hat{g}_{i,k}^{est}$ and $\hat{g}_{i,k}$ denote the estimated and real channels between the k-th RIS element and the i-th receive antenna of RIS-SM, respectively, and $n_{i,k}$ denotes a Gaussian random variable with zero mean and δ_e variance. It is observed from Fig. 17 that RIS-JIK-MDCSK with imperfect IPE has about 1 dB penalty in BER performance in contrast to that with perfect IPE. However, RIS-JIK-MDCSK with imperfect IPE outperforms RIS-SSK and RIS-SM with perfect CSI by more than 3 dB and 4 dB, respectively. Therefore, the proposed non-coherent RIS-JIK-MDCSK system is more suitable for communication scenarios where obtaining CSI and IPE is challenging, such as high-speed mobile scenarios.

Remark 3: The RIS deployed at the transmitter enables the proposed RIS-JIK-MDCSK system to achieve better BER performance compared to other DCSK-based systems even under the condition that the RIS has one element. When the number of RIS elements, N, is large, the RIS-JIK-MDCSK system can achieve a better BER performance. The proposed non-coherent RIS-JIK-MDCSK system outperforms the coherent RIS-SM system for different modulation orders and numbers of RIS elements. If RIS-SM utilizes ML decoding, CSI is necessary to find one of the combinations of different antennas and M-PSK symbols to retrieve the information bits, which results in a high computational complexity. In contrast, the proposed RIS-JIK-MDCSK system performs non-coherent detection that dispenses with the CSI, thus reducing the system complexity.

VI. Conclusion

To prevent the excessive system overhead of coherent RIS-aided communication systems imposed by channel estimation, we have proposed a non-coherent RIS-aided M-ary differential chaos shift keying system to offer superior BER performance without the need for CSI. In the proposed RIS-JIK-MDCSK system, the reference signal is used to transmit one information bit by using the index of the selected reference signal, therefore reducing the energy consumption and increasing the data rate. Furthermore, the reference keying, RIS keying, and carrier keying have been jointly designed to achieve high-data-rate transmission, where extra information bits are carried by the indices of these keying entities. In order to recover the information bits transmitted by different keying indices and the physically modulated M-ary constellation symbol, we have proposed an effective joint index keying algorithm. The BER performance, throughput, spectral efficiency, and system complexity of RIS-JIK-MDCSK have been analyzed and have been compared to relevant benchmark systems. It has been demonstrated with the aid of simulations that the proposed RIS-JIK-MDCSK system is capable of achieving superior throughput, spectral efficiency, and BER performance compared to other systems at the cost of an increased system complexity. Specifically, the proposed non-coherent RIS-JIK-MDCSK system can obtain comparable and even superior BER performance compared to the coherent RIS-SM system. Therefore, the proposed RIS-JIK-MDCSK system is a promising non-coherent system for future wireless communications. Our future efforts will be devoted to studying mutiple RIS-assisted non-coherent communications.

Acknowledgment

Any opinions, findings and conclusions or recommendations expressed in this material are those of the author(s) and do not reflect the views of the Singapore Ministry of Education.

References

[1] M. Di Renzo et al., "Smart radio environments empowered by reconfigurable intelligent surfaces: How it works, state of research, and the road ahead," *IEEE J. Sel. Areas Commun.*, vol. 38, no. 11, pp. 2450–2525, Nov. 2020.

[2] C. Huang, A. Zappone, G. C. Alexandropoulos, M. Debbah, and C. Yuen, "Reconfigurable intelligent surfaces for energy efficiency in wireless communication," *IEEE Trans. Wireless Commun.*, vol. 18, no. 8, pp. 4157–4170, Aug. 2019.

[3] Q. Wu and R. Zhang, "Intelligent reflecting surface enhanced wireless network via joint active and passive beamforming," *IEEE Trans. Wireless Commun.*, vol. 18, no. 11, pp. 5394–5409, Nov. 2019.

[4] C. Huang et al., "Holographic MIMO surfaces for 6G wireless networks: Opportunities, challenges, and trends," *IEEE Wireless Commun.*, vol. 27, no. 5, pp. 118–125, Oct. 2020.

[5] W. Tang et al., "Wireless communications with reconfigurable intelligent surface: Path loss modeling and experimental measurement," *IEEE Trans. Wireless Commun.*, vol. 20, no. 1, pp. 421–439, Jan. 2021.

[6] Q. Wu and R. Zhang, "Towards smart and reconfigurable environment: Intelligent reflecting surface aided wireless network," *IEEE Commun. Mag.*, vol. 58, no. 1, pp. 106–112, Jan. 2020.

[7] E. Basar, M. Di Renzo, J. De Rosny, M. Debbah, M. Alouini, and R. Zhang, "Wireless communications through reconfigurable intelligent surfaces," *IEEE Access*, vol. 7, pp. 116753–116773, 2019.

[8] E. Basar, "Transmission through large intelligent surfaces: A new frontier in wireless communications," in *Proc. Eur. Conf. Netw. Commun. (EuCNC)*, Jun. 2019, pp. 112–117.

[9] E. Basar, "Reconfigurable intelligent surface-based index modulation: A new beyond MIMO paradigm for 6G," *IEEE Trans. Commun.*, vol. 68, no. 5, pp. 3187–3196, May 2020.

[10] S. Luo et al., "Spatial modulation for RIS-assisted uplink communication: Joint power allocation and passive beamforming design," *IEEE Trans. Commun.*, vol. 69, no. 10, pp. 7017–7031, Oct. 2021.

[11] S. Gopi, S. Kalyani, and L. Hanzo, "Intelligent reflecting surface assisted beam index-modulation for millimeter wave communication," *IEEE Trans. Wireless Commun.*, vol. 20, no. 2, pp. 983–996, Feb. 2021.

[12] M. H. Dinan, N. S. Perović, and M. F. Flanagan, "RIS-assisted receive quadrature space-shift keying: A new paradigm and performance analysis," *IEEE Trans. Commun.*, vol. 70, no. 10, pp. 6874–6889, Oct. 2022.

[13] K. Asmoro and S. Y. Shin, "RIS grouping based index modulation for 6G telecommunications," *IEEE Wireless Commun. Lett.*, vol. 11, no. 11, pp. 2410–2414, Nov. 2022.

[14] L. Wei, C. Huang, G. C. Alexandropoulos, C. Yuen, Z. Zhang, and M. Debbah, "Channel estimation for RIS-empowered multi-user MISO wireless communications," *IEEE Trans. Commun.*, vol. 69, no. 6, pp. 4144–4157, Jun. 2021.

[15] Z. Wang, L. Liu, and S. Cui, "Channel estimation for intelligent reflecting surface assisted multiuser communications: Framework, algorithms, and analysis," *IEEE Trans. Wireless Commun.*, vol. 19, no. 10, pp. 6607–6620, Oct. 2020.

[16] J. G. Lawton, "Theoretical error rates of 'differentially coherent' binary and 'Kineplex' data transmission systems," *Proc. IRE*, vol. 47, no. 2, pp. 333–334, 1959.

[17] M. Chowdhury, A. Manolakos, and A. Goldsmith, "Scaling laws for noncoherent energy-based communications in the SIMO MAC," *IEEE Trans. Inf. Theory*, vol. 62, no. 4, pp. 1980–1992, Apr. 2016.

[18] G. Kolumbán, G. K. Vizvari, W. Schwarz, and A. Abel, "Differential chaos shift keying: A robust coding for chaos communication," in *Proc. Nonlinear Dyn. Electron. Syst.*, Seville, Spain, 1996, pp. 92–97.

[19] F. J. Escribano, G. Kaddoum, A. Wagemakers, and P. Giard, "Design of a new differential chaos-shift-keying system for continuous mobility," *IEEE Trans. Commun.*, vol. 64, no. 5, pp. 2066–2078, May 2016.

[20] H. Ma, G. Cai, Y. Fang, J. Wen, P. Chen, and S. Akhtar, "A new enhanced energy-detector-based FM-DCSK UWB system for tactile internet," *IEEE Trans. Ind. Informat.*, vol. 15, no. 5, pp. 3028–3039, May 2019.

[21] R. Luo, H. Yang, C. Meng, and X. Zhang, "A novel SR-DCSK-based ambient backscatter communication system," *IEEE Trans. Circuits Syst. II, Exp. Briefs*, vol. 69, no. 3, pp. 1707–1711, Mar. 2022.

[22] G. Cai, Y. Fang, P. Chen, G. Han, G. Cai, and Y. Song, "Design of an MISO-SWIPT-aided code-index modulated multi-carrier M-DCSK system for e-Health IoT," *IEEE J. Sel. Areas Commun.*, vol. 39, no. 2, pp. 311–324, Feb. 2021.

[23] Z. Chen, L. Zhang, J. Zhang, Z. Wu, and D. Luobu, "An OFDM-based pre-coded chaos shift keying transceiver for reliable V2V transmission," *IEEE Trans. Veh. Technol.*, vol. 71, no. 6, pp. 6710–6715, Jun. 2022.

[24] M. Miao, L. Wang, G. Chen, and W. Xu, "Design and analysis of replica piecewise M-ary DCSK scheme for power line communications with asynchronous impulsive noise," *IEEE Trans. Circuits Syst. I, Reg. Papers*, vol. 67, no. 12, pp. 5443–5453, Dec. 2020.

[25] X. Cai, W. Xu, L. Wang, and G. Kaddoum, "Joint energy and correlation detection assisted non-coherent OFDM-DCSK system for underwater acoustic communications," *IEEE Trans. Commun.*, vol. 70, no. 6, pp. 3742–3759, Jun. 2022.

[26] G. Kaddoum, F.-D. Richardson, and F. Gagnon, "Design and analysis of a multi-carrier differential chaos shift keying communication system," *IEEE Trans. Commun.*, vol. 61, no. 8, pp. 3281–3291, Aug. 2013.

[27] X. Cai, W. Xu, S. Hong, and L. Wang, "A trinal-code shifted differential chaos shift keying system," *IEEE Commun. Lett.*, vol. 25, no. 3, pp. 1000–1004, Mar. 2021.

[28] H. Zhang, L. Zhang, Y. Jiang, and Z. Wu, "Reliable and secure deep learning-based OFDM-DCSK transceiver design without delivery of reference chaotic sequences," *IEEE Trans. Veh. Technol.*, vol. 71, no. 8, pp. 8059–8074, Aug. 2022.

[29] B. Chen, L. Zhang, and Z. Wu, "General iterative receiver design for enhanced reliability in multi-carrier differential chaos shift keying systems," *IEEE Trans. Commun.*, vol. 67, no. 11, pp. 7824–7839, Nov. 2019.

[30] X. Cai, W. Xu, L. Wang, and G. Kolumbán, "Design and performance analysis of a robust multi-carrier M-ary DCSK system: A noise suppression perspective," *IEEE Trans. Commun.*, vol. 70, no. 3, pp. 1623–1637, Mar. 2022.

[31] H. Yang, G.-P. Jiang, W. K. S. Tang, G. Chen, and Y.-C. Lai, "Multi-carrier differential chaos shift keying system with subcarriers allocation for noise reduction," *IEEE Trans. Circuits Syst. II, Exp. Briefs*, vol. 65, no. 11, pp. 1733–1737, Nov. 2018.

[32] E. Başar, "Index modulation techniques for 5G wireless networks," *IEEE Commun. Mag.*, vol. 54, no. 7, pp. 168–175, Jul. 2016.

[33] E. Basar, M. Wen, R. Mesleh, M. Di Renzo, Y. Xiao, and H. Haas, "Index modulation techniques for next-generation wireless networks," *IEEE Access*, vol. 5, pp. 16693–16746, 2017.

[34] G. Cheng, L. Wang, W. Xu, and G. Chen, "Carrier index differential chaos shift keying modulation," *IEEE Trans. Circuits Syst. II, Exp. Briefs*, vol. 64, no. 8, pp. 907–911, Aug. 2017.

[35] G. Cheng, X. Chen, W. Liu, and W. Xiao, "GCI-DCSK: Generalized carrier index differential chaos shift keying modulation," *IEEE Commun. Lett.*, vol. 23, no. 11, pp. 2012–2016, Nov. 2019.

[36] G. Cheng, L. Wang, Q. Chen, and G. Chen, "Design and performance analysis of generalised carrier index M-ary differential chaos shift keying modulation," *IET Commun.*, vol. 12, no. 11, pp. 1324–1331, Jul. 2018.

[37] G. Cai, Y. Fang, J. Wen, S. Mumtaz, Y. Song, and V. Frascolla, "Multi-carrier M-ary DCSK system with code index modulation: An efficient solution for chaotic communications," *IEEE J. Sel. Topics Signal Process.*, vol. 13, no. 6, pp. 1375–1386, Oct. 2019.

[38] H. Chen, P. Chen, Y. Fang, F. Chen, and L. Kong, "Parallel differential chaotic shift keying with code index modulation for wireless communication," *IEEE Trans. Commun.*, vol. 70, no. 8, pp. 5113–5127, Aug. 2022.

[39] M. Herceg, G. Kaddoum, D. Vranješ, and E. Soujeri, "Permutation index DCSK modulation technique for secure multiuser high-data-rate communication systems," *IEEE Trans. Veh. Technol.*, vol. 67, no. 4, pp. 2997–3011, Apr. 2018.

[40] H. Chen, P. Chen, S. Wang, S. Lai, and R. Chen, "Reference-modulated PI-DCSK: A new efficient chaotic permutation index modulation scheme," *IEEE Trans. Veh. Technol.*, vol. 71, no. 9, pp. 9663–9673, Sep. 2022.

[41] X. Cai, W. Xu, S. Hong, and L. Wang, "Dual-mode differential chaos shift keying with index modulation," *IEEE Trans. Commun.*, vol. 67, no. 9, pp. 6099–6111, Sep. 2019.

[42] X. Cai, W. Xu, S. Hong, L. Wang, and L. Zhang, "General carrier index aided dual-mode differential chaos shift keying with full mapping: Design and optimization," *IEEE Trans. Veh. Technol.*, vol. 70, no. 11, pp. 11665–11677, Nov. 2021.

[43] H. Ma, Y. Fang, Y. Tao, P. Chen, and Y. Li, "A novel differential chaos shift keying scheme with transmit diversity," *IEEE Commun. Lett.*, vol. 26, no. 1, pp. 1668–1672, Jul. 2022.

[44] Y. Tao, Y. Fang, H. Ma, S. Mumtaz, and M. Guizani, "Multi-carrier DCSK with hybrid index modulation: A new perspective on frequency-index-aided chaotic communication," *IEEE Trans. Commun.*, vol. 70, no. 6, pp. 3760–3773, Jun. 2022.

[45] H. Ma, Y. Fang, P. Chen, S. Mumtaz, and Y. Li, "A novel differential chaos shift keying scheme with multidimensional index modulation," *IEEE Trans. Wireless Commun.*, vol. 22, no. 1, pp. 237–256, Jan. 2023, doi: 10.1109/TWC.2022.3192347.

[46] G. Kaddoum, P. Chargé, D. Roviras, and D. Fournier-Prunaret, "A methodology for bit error rate prediction in chaos-based communication systems," *Circuits, Syst. Signal Process.*, vol. 28, no. 6, pp. 925–944, Aug. 2009.

[47] W. M. Tam, F. C. M. Lau, C. K. Tse, and A. J. Lawrance, "Exact analytical bit error rates for multiple access chaos-based communication systems," *IEEE Trans. Circuits Syst. II, Exp. Briefs*, vol. 51, no. 9, pp. 473–481, Sep. 2004.

[48] V. Cizek, "Discrete Hilbert transform," *IEEE Trans. Audio Electroacoust.*, vol. AU-18, no. 4, pp. 340–343, Dec. 1970.

[49] E. Başar, U. Aygölü, E. Panayırcı, and H. V. Poor, "Orthogonal frequency division multiplexing with index modulation," *IEEE Trans. Signal Process.*, vol. 61, no. 22, pp. 5536–5549, Nov. 2013.

[50] A. Papoulis and U. Pillai, *Probability, Random Variables and Stochastic Processes*, 4th ed. New York, NY, USA: McGraw-Hill, Nov. 2001.

[51] A. Sendonaris, E. Erkip, and B. Aazhang, "User cooperation diversity—Part I: System description," *IEEE Trans. Commun.*, vol. 51, no. 11, pp. 1927–1938, Nov. 2003.

[52] G. Cai, Y. Fang, G. Han, J. Xu, and G. Chen, "Design and analysis of relay-selection strategies for two-way relay network-coded DCSK systems," *IEEE Trans. Veh. Technol.*, vol. 67, no. 2, pp. 1258–1271, Feb. 2018.

[53] S. Benedetto and E. Biglieri, *Principles of Digital Transmission: With Wireless Applications*. Norwell, MA, USA: Kluwer, 1999.

[54] H. Yang, W. K. S. Tang, G. Chen, and G.-P. Jiang, "Multi-carrier chaos shift keying: System design and performance analysis," *IEEE Trans. Circuits Syst. I, Reg. Papers*, vol. 64, no. 8, pp. 2182–2194, Aug. 2017.

Xiangming Cai (Member, IEEE) received the B.Eng. degree in information engineering from the Guangdong University of Technology, Guangzhou, China, in 2017, and the Ph.D. degree in communication and information systems from Xiamen University, Xiamen, China, in 2021. Since 2022, he has been a Research Fellow with the Engineering Product Development Pillar, Singapore University of Technology and Design. His research interests include wireless communications, reconfigurable intelligent surfaces, chaotic communications, and underwater acoustic communications. He was a recipient of the Best Paper Award of the 2021 IEEE Asia–Pacific Conference on Communications. He was also a recipient of an Exemplary Reviewer of the IEEE TRANSACTIONS ON COMMUNICATIONS.

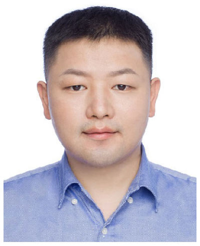

Chongwen Huang (Member, IEEE) received the B.Sc. degree from Nankai University in 2010, the M.Sc. degree from the University of Electronic Science and Technology of China in 2013, and the Ph.D. degree from the Singapore University of Technology and Design (SUTD) in 2019. From October 2019 to September 2020, he was a Post-Doctoral Researcher with SUTD. In September 2020, he joined Zhejiang University, as a tenure-track Young Professor. His main research interests are focused on holographic MIMO surface/reconfigurable intelligent surface, B5G/6G wireless communication, mmWave/THz communications, and deep learning technologies for wireless communications. He was a recipient of the IEEE Marconi Prize Paper Award in Wireless Communications and the IEEE ComSoc Asia–Pacific Outstanding Young Researcher Award in 2021. He has been serving as an Editor for IEEE COMMUNICATIONS LETTERS, *Signal Processing* (Elsevier), and *EURASIP Journal on Wireless Communications and Networking and Physical Communication*, since 2021.

Ertugrul Basar (Fellow, IEEE) received the Ph.D. degree from Istanbul Technical University in 2013. He is currently an Associate Professor with the Department of Electrical and Electronics Engineering, Koç University, Istanbul, Turkey; and the Director of the Communications Research and Innovation Laboratory (CoreLab). He has visiting positions with Ruhr University Bochum, Germany, in 2022 as a Mercator Fellow; and Princeton University, USA, from 2011 to 2012, as a Visiting Research Collaborator. He is the author/coauthor of around 130 international journal publications and ten patents that received more than 10,000 citations. His primary research interests include beyond 5G and 6G wireless networks, communication theory and systems, reconfigurable intelligent surfaces, index modulation, waveform design, and signal processing for communications. He has been a Young Member of Turkish Academy of Sciences since 2017. In the past, he served as an Editor/a Senior Editor for many journals, including IEEE COMMUNICATIONS LETTERS (2016–2022), IEEE TRANSACTIONS ON COMMUNICATIONS (2018–2022), *Physical Communication* (2017–2020), and IEEE ACCESS (2016–2018). Currently, he is an Editor of *Frontiers in Communications and Networks*.

Weikai Xu (Member, IEEE) received the B.S. degree in electronic engineering from Three Gorges College, Chongqing, China, in 2000, the M.Sc. degree in communication and information system from the Chongqing University of Posts and Telecommunications, Chongqing, in 2003, and the Ph.D. degree in electronic circuit and system from the Xiamen University of China, Xiamen, China, in 2011. From 2003 to 2012, he was a Teaching Assistant and an Assistant Professor with the Department of Communication Engineering, Xiamen University, where he is currently an Associate Professor with the Department of Information and Communication Engineering. His current research interests include chaos-based digital communications and underwater acoustic communications.

Lin Wang (Senior Member, IEEE) received the Ph.D. degree in electronics engineering from the University of Electronic Science and Technology of China, Chengdu, China, in 2001. From 1984 to 1986, he was a Teaching Assistant with the Mathematics Department, Chongqing Normal University. From 1989 to 2002, he was a Teaching Assistant, a Lecturer, and then an Associate Professor of applied mathematics and communication engineering with the Chongqing University of Post and Telecommunication, Chongqing, China. From 1995 to 1996, he was with the Mathematics Department, University of New England, Armidale, NSW, Australia. In 2003, he spent three months as a Visiting Researcher with the Center for Chaos and Complexity Networks, City University of Hong Kong. In 2013, he was a Senior Visiting Researcher with the Department of Electrical and Computer Engineering (ECE), University of California at Davis, CA, USA. He was a Distinguished Professor with Xiamen University, China, from 2012 to 2017, where he has been a Full Professor with the School of Informatics, since 2003. He has authored more than 250 journals and conference papers (including 92 IEEE journal articles and four best paper awards). He holds 21 patents in physical layer in digital communications. His current research interests include source coding/channel coding, joint source and channel coding/decoding, chaos modulation and their applications to wired/wireless communication, power line communication (PLC), and underwater acoustic communications (UAC). He has host some international conferences as the general chair and the TPC chair in his career. Meanwhile, he has also delivered some plenary/keynote speeches in the international conferences in recent several years.

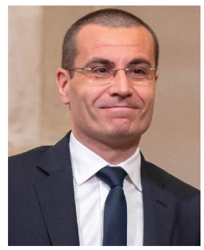

Marco Di Renzo (Fellow, IEEE) received the Laurea (cum laude) and Ph.D. degrees in electrical engineering from the University of L'Aquila, Italy, in 2003 and 2007, respectively, and the Habilitation à Diriger des Recherches (Doctor of Science) degree from University Paris-Sud (currently Paris-Saclay University), France, in 2013. Currently, he is a CNRS Research Director (Professor) and the Head of the Intelligent Physical Communications Group, Laboratory of Signals and Systems (L2S), CNRS and CentraleSupélec, Paris-Saclay University, Paris, France. In Paris-Saclay University, he serves as the Coordinator of the communications and networks research area with the Laboratory of Excellence DigiCosme and a member of the Admission and Evaluation Committee of the Ph.D. School on Information and Communication Technologies and a member of the Evaluation Committee of the Graduate School in Computer Science. He is a Founding Member and the Academic Vice Chair of the Industry Specification Group (ISG) on Reconfigurable Intelligent Surfaces (RIS), European Telecommunications Standards Institute (ETSI), where he serves as the Rapporteur for the work item on communication models, channel models, and evaluation methodologies. He is a fellow of IET, and AAIA; an Ordinary Member of the European Academy of Sciences and Arts and the Academia Europaea; and a Highly Cited Researcher. Also, he is a Fulbright Fellow at the City University of New York, USA. He was a Nokia Foundation Visiting Professor and a Royal Academy of Engineering Distinguished Visiting Fellow. His recent research awards include the 2021 EURASIP Best Paper Award, the 2022 IEEE COMSOC Outstanding Paper Award, the 2022 Michel Monpetit Prize conferred by the French Academy of Sciences, the 2023 EURASIP Best Paper Award, the 2023 IEEE COMSOC Fred W. Ellersick Prize, and the 2023 IEEE COMSOC Heinrich Hertz Award. He serves as the Editor-in-Chief for IEEE COMMUNICATIONS LETTERS.

Chau Yuen (Fellow, IEEE) received the B.Eng. and Ph.D. degrees from Nanyang Technological University, Singapore, in 2000 and 2004, respectively.

He was a Post-Doctoral Fellow with Lucent Technologies Bell Labs, Murray Hill, in 2005, and a Visiting Assistant Professor with The Hong Kong Polytechnic University in 2008. From 2006 to 2010, he was with the Institute for Infocomm Research, Singapore. From 2010 to 2023, he was a Associate Professor with the Engineering Product Development Pillar, Singapore University of Technology and Design. Since 2023, he has been with the School of Electrical and Electronic Engineering, Nanyang Technological University. He has three U.S. patents and published over 500 research papers at international journals or conferences.

Dr. Yuen was a recipient of the Lee Kuan Yew Gold Medal, the Institution of Electrical Engineers Book Prize, the Institute of Engineering of Singapore Gold Medal, the Merck Sharp and Dohme Gold Medal, and the Hewlett Packard Prize (twice). He received the IEEE Asia–Pacific Outstanding Young Researcher Award in 2012 and the IEEE VTS Singapore Chapter Outstanding Service Award on 2019. He serves as an Editor for IEEE TRANSACTIONS ON VEHICULAR TECHNOLOGY, IEEE SYSTEMS JOURNAL, and IEEE TRANSACTIONS ON NETWORK SCIENCE AND ENGINEERING, where he was awarded as an IEEE TRANSACTIONS ON NETWORK SCIENCE AND ENGINEERING Excellent Editor Award and the Top Associate Editor for IEEE TRANSACTIONS ON VEHICULAR TECHNOLOGY, from 2009 to 2015. He also served as the Guest Editor for several special issues, including IEEE JOURNAL ON SELECTED AREAS IN COMMUNICATIONS, *IEEE Wireless Communications Magazine*, *IEEE Communications Magazine*, *IEEE Vehicular Technology Magazine*, IEEE TRANSACTIONS ON COGNITIVE COMMUNICATIONS AND NETWORKING, and *Applied Energy* (Elsevier). He is a Distinguished Lecturer of IEEE Vehicular Technology Society and also a Highly Cited Researcher by Clarivate Web of Science.